nature metabolism

ARTICLES

https://doi.org/10.1038/s42255-018-0007-6

Interaction between hormone-sensitive lipase and ChREBP in fat cells controls insulin sensitivity

Pauline Morigny[1,2,26], Marianne Houssier[1,2,26], Aline Mairal[1,2], Claire Ghilain[1,2], Etienne Mouisel[1,2], Fadila Benhamed[3,4,5], Bernard Masri[1,2], Emeline Recazens[1,2], Pierre-Damien Denechaud[1,2], Geneviève Tavernier[1,2], Sylvie Caspar-Bauguil[1,2,6], Sam Virtue[7], Veronika Sramkova[1,2,8,9], Laurent Monbrun[1,2], Anne Mazars[1,2], Madjid Zanoun[1,2], Sandra Guilmeau[3,4,5], Valentin Barquissau[1,2], Diane Beuzelin[1,2], Sophie Bonnel[1,2,9], Marie Marques[1,2,9], Boris Monge-Roffarello[1,2], Corinne Lefort[1,2], Barbara Fielding[10], Thierry Sulpice[11], Arne Astrup[12], Bernard Payrastre[1,2], Justine Bertrand-Michel[1,2], Emmanuelle Meugnier[13], Laetitia Ligat[14], Frédéric Lopez[14], Hervé Guillou[15,16], Charlotte Ling[17], Cecilia Holm[18], Remi Rabasa-Lhoret[19,20,21], Wim H. M. Saris[22], Vladimir Stich[8,9], Peter Arner[23], Mikael Rydén[23], Cedric Moro[1,2,9], Nathalie Viguerie[1,2,9], Matthew Harms[24], Stefan Hallén[24], Antonio Vidal-Puig[7,25], Hubert Vidal[13], Catherine Postic[3,4,5] and Dominique Langin[1,2,6,9]*

Impaired adipose tissue insulin signalling is a critical feature of insulin resistance. Here we identify a pathway linking the lipolytic enzyme hormone-sensitive lipase (HSL) to insulin action via the glucose-responsive transcription factor ChREBP and its target, the fatty acid elongase ELOVL6. Genetic inhibition of HSL in human adipocytes and mouse adipose tissue results in enhanced insulin sensitivity and induction of ELOVL6. ELOVL6 promotes an increase in phospholipid oleic acid, which modifies plasma membrane fluidity and enhances insulin signalling. HSL deficiency–mediated effects are suppressed by gene silencing of ChREBP and ELOVL6. Mechanistically, physical interaction between HSL, independent of lipase activity, and the isoform activated by glucose metabolism ChREBPα impairs ChREBPα translocation into the nucleus and induction of ChREBPβ, the isoform with high transcriptional activity that is strongly associated with whole-body insulin sensitivity. Targeting the HSL–ChREBP interaction may allow therapeutic strategies for the restoration of insulin sensitivity.

Insulin resistance is a pathogenic mechanism involved in a wide array of diseases. The importance of adipose tissue metabolism as a determinant of systemic insulin sensitivity has been shown in transgenic mouse models[1–4] and clinical studies[5–8]. In this context, improvement of adipose tissue insulin action seems to be an important target for recovery of whole-body systemic insulin sensitivity. Excessive circulating levels of fatty acids are important contributors to insulin resistance through development of fatty acid–induced lipotoxicity in insulin-sensitive tissues[9]. Lowering plasma nonesterified fatty acid levels through inhibition of fat cell lipolysis has been proposed as a way to improve insulin sensitivity. However, human data call into question the association between production of fatty acids from adipose tissue lipolysis and insulin resistance in obesity[10]. Partial deficiency in hormone-sensitive lipase (HSL, encoded by *LIPE*), one of the neutral lipases expressed in adipocytes, results in greater whole-body insulin sensitivity in obese mice without changes in plasma fatty acid levels[11].

[1]Institut National de la Santé et de la Recherche Médicale (Inserm), UMR1048, Institute of Metabolic and Cardiovascular Diseases, Toulouse, France. [2]University of Toulouse, UMR1048, Institute of Metabolic and Cardiovascular Diseases, Paul Sabatier University, Toulouse, France. [3]Institut National de la Santé et de la Recherche Médicale (Inserm), U1016, Institut Cochin, Paris, France. [4]Centre National de la Recherche Scientifique (CNRS), UMR 8104, Paris, France. [5]Université Paris Descartes, Sorbonne Paris Cité, Paris, France. [6]Toulouse University Hospitals, Laboratory of Clinical Biochemistry, Toulouse, France. [7]University of Cambridge Metabolic Research Laboratories, Wellcome Trust-MRC Institute of Metabolic Science, Addenbrooke's Hospital, Cambridge, UK. [8]Department for the Study of Obesity and Diabetes, Third Faculty of Medicine, Charles University, Prague, Czech Republic. [9]Franco-Czech Laboratory for Clinical Research on Obesity, Third Faculty of Medicine, Prague and Paul Sabatier University, Toulouse, France. [10]Department of Nutritional Sciences, University of Surrey, Guildford, Surrey, UK. [11]Physiogenex SAS, Prologue Biotech, Labège, France. [12]Department of Nutrition, Exercise and Sports, Faculty of Science, University of Copenhagen, Copenhagen, Denmark. [13]CarMeN Laboratory, Inserm U1060, INRA U1397, Université Lyon 1, INSA Lyon, Oullins, France. [14]Pôle Technologique, Cancer Research Center of Toulouse (CRCT), Plateau Interactions Moléculaires, INSERM-UMR1037, Toulouse, France. [15]Institut National de la Recherche Agronomique (INRA), UMR1331, Integrative Toxicology and Metabolism, Toulouse, France. [16]University of Toulouse, UMR1331, Institut National Polytechnique (INP), Paul Sabatier University, Toulouse, France. [17]Department of Clinical Sciences, Epigenetics and Diabetes, Lund University Diabetes Centre, Clinical Research Centre, Malmö, Sweden. [18]Department of Experimental Medical Science, Lund University, Biomedical Centre, Lund, Sweden. [19]Institut de Recherches Cliniques de Montréal, Montreal, Canada. [20]Department of nutrition, Université de Montréal, Montreal, Canada. [21]Montreal Diabetes Research Center (MDRC), Montreal, Canada. [22]Department of Human Biology, NUTRIM School of Nutrition and Translational Research in Metabolism, Maastricht University Medical Centre, Maastricht, the Netherlands. [23]Department of Medicine, H7, Karolinska Institutet and Karolinska University Hospital, Huddinge, Stockholm, Sweden. [24]Cardiovascular, Renal and Metabolism, IMED Biotech Unit, AstraZeneca, Gothenburg, Sweden. [25]Wellcome Trust Sanger Institute, Wellcome Trust Genome Campus, Hinxton, Cambridgeshire, UK. [26]These authors contributed equally: P. Morigny, M. Houssier. *e-mail: dominique.langin@inserm.fr

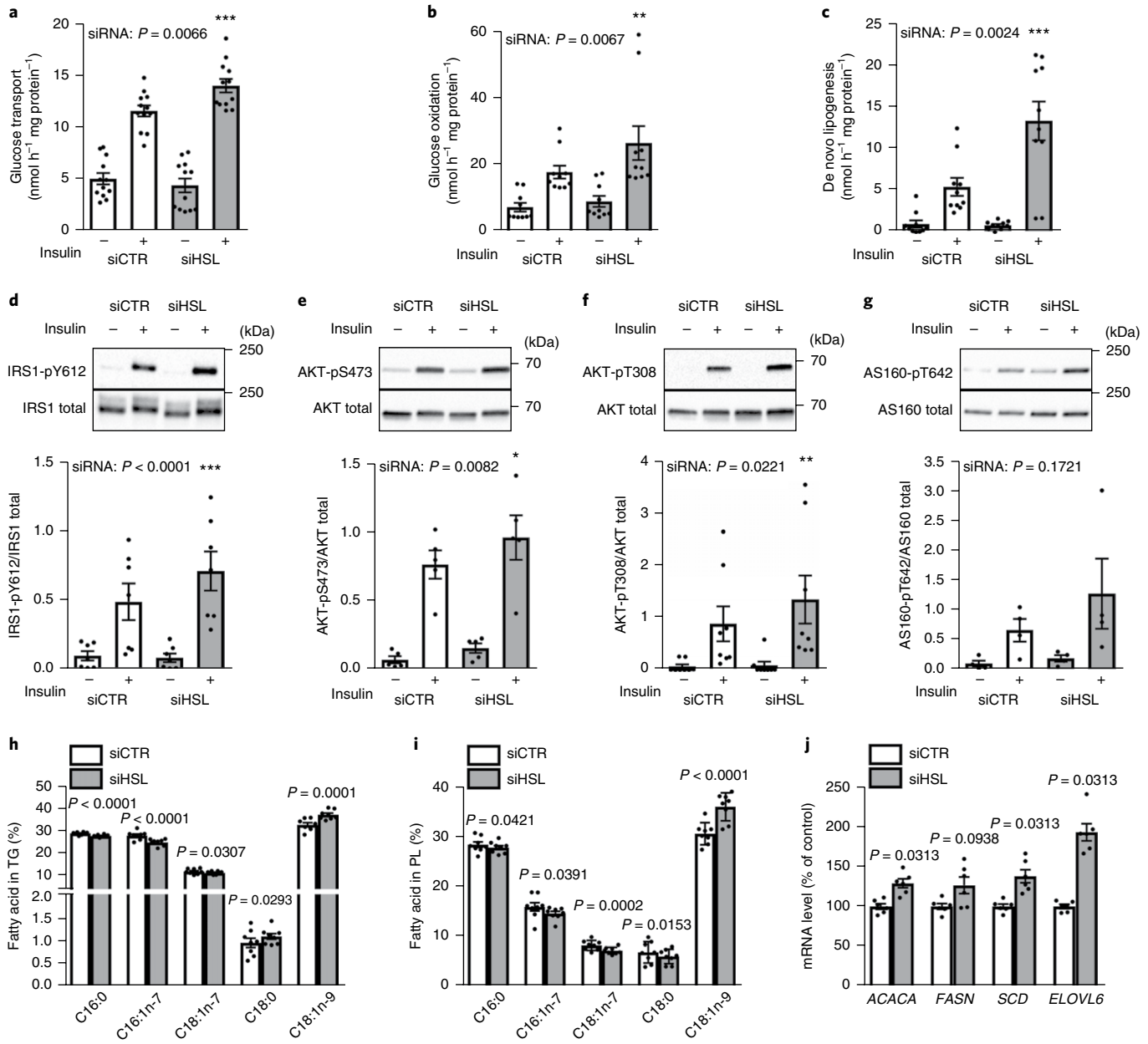

Fig. 1 | Reduced HSL expression promotes glucose metabolism and insulin signalling in human adipocytes. Experiments were carried out in control (white bars, siCTR) and HSL-deprived (grey bars, siHSL) hMADS adipocytes. **a**–**g**, Adipocytes were analyzed in basal (–) and insulin-stimulated (+, 100 nM) conditions. **a**, Glucose transport using radiolabelled 2-deoxyglucose ($n = 12$ biologically independent samples per group). Insulin stimulation: $P < 0.0001$. **b**, Glucose oxidation using radiolabelled glucose ($n = 10$ biologically independent samples per group). Insulin stimulation: $P = 0.0015$. **c**, DNL using radiolabelled glucose ($n = 10$ biologically independent samples per group). Insulin stimulation: $P < 0.0001$. **d**–**g**, Insulin signalling evaluated by activating phosphorylation of IRS1 (pY612) ($n = 7$ biologically independent samples per group; insulin stimulation: $P = 0.0033$) (**d**); AKT (pS473) ($n = 5$ biologically independent samples per group; insulin stimulation: $P = 0.0005$) (**e**); AKT (pT308) ($n = 8$ biologically independent samples per group; insulin stimulation: $P = 0.0201$) (**f**); and AS160 (pT642) ($n = 4$ biologically independent samples per group ; insulin stimulation: $P = 0.0726$) (**g**). Size markers (in kDa) are shown on illustrative western blot panels. **h**,**i**, Fatty acid composition (C16:0, palmitic acid; C16:1n-7, palmitoleic acid; C18:1n-7; vaccenic acid; C18:0, stearic acid; C18:1n-9, oleic acid) in triglycerides (TG) (**h**) and phospholipids (PL) (**i**) ($n = 8$ biologically independent samples per group). **j**, mRNA levels of lipogenic enzymes ($n = 6$ biologically independent samples per group). Data are mean ± s.e.m. Statistical analysis was performed using two-way analysis of variance (ANOVA) with Bonferroni's post hoc tests (**a**–**g**), paired Student's *t*-test (**h**,**i**) and Wilcoxon's test (**j**). Statistical tests were two-sided. $^*P < 0.05$, $^{**}P < 0.01$, $^{***}P < 0.001$ compared to control.

Here, in a series of in vitro and in vivo studies in humans and mice, we identified a pathway linking HSL to insulin resistance through interaction with the glucose-responsive transcription factor ChREBP. The physical interaction between HSL and ChREBP impairs nuclear translocation and activity of the transcription factor. In fat cells, the lipogenic enzyme ELOVL6 is a preferential target of ChREBP. Inhibition of HSL promotes activity of ELOVL6 and enhances insulin signalling through enrichment of plasma membrane phospholipids in oleic acid.

Results

Reduced adipocyte HSL expression favors glucose metabolism. In adipocytes differentiated from human multipotent adipose-derived

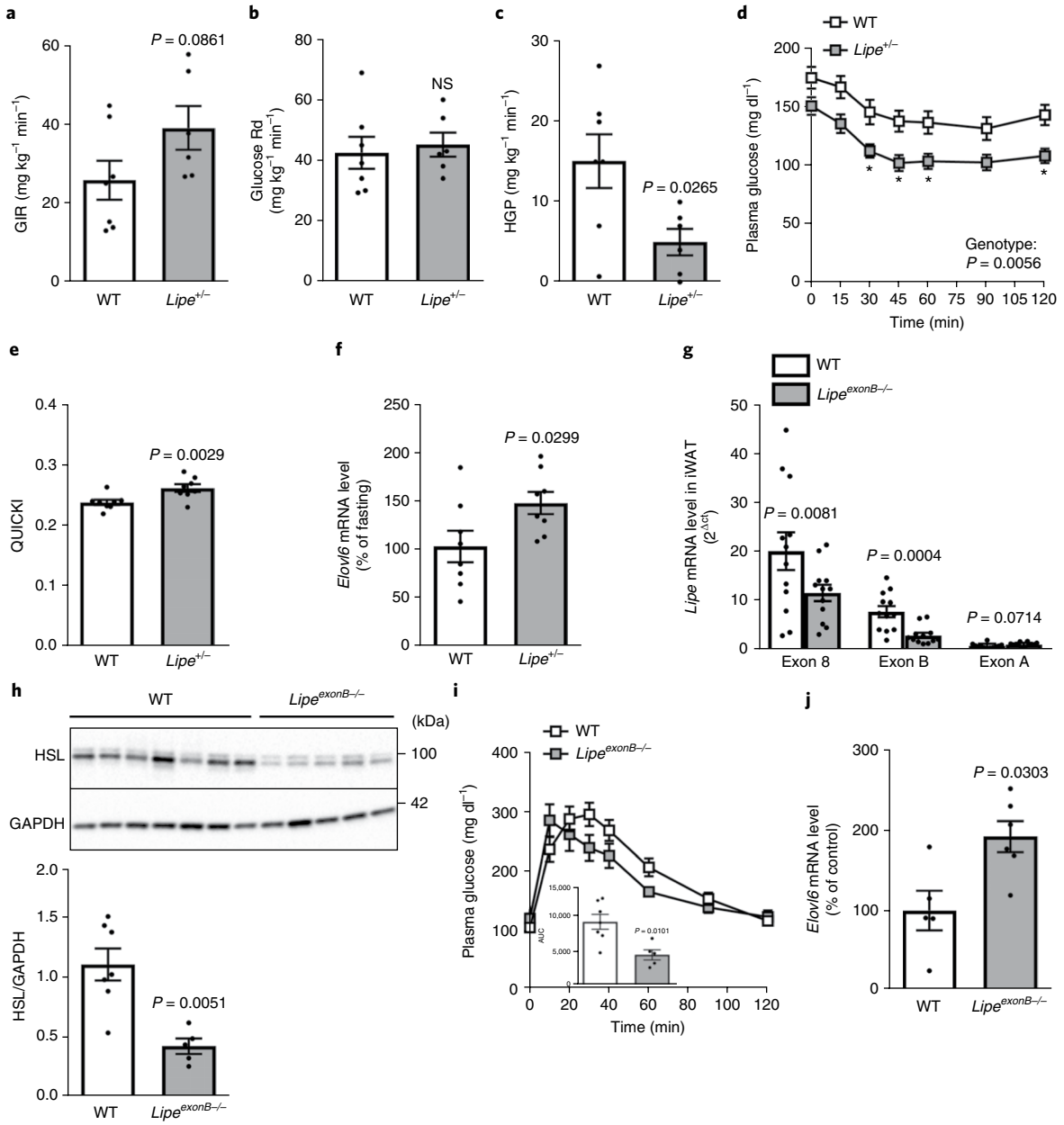

Fig. 2 | HSL inhibition is associated with increased insulin sensitivity and adipose tissue ELOVL6 expression in vivo. a–f, Experiments were carried out in wild-type (WT, white bars) and HSL haploinsufficient (*Lipe*$^{+/-}$, grey bars) mice. **a–c**, Glucose infusion rate (GIR) (**a**), post-insulin rate of glucose disappearance (Glucose Rd) (**b**), and hepatic glucose production (HGP) (**c**) during euglycemic-hyperinsulinemic clamp in B6D2/F1 mice fed 60% high-fat diet for 3 months (WT $n=7$ animals, *Lipe*$^{+/-}$ $n=6$ animals). **d**, Plasma glucose concentration during an insulin tolerance test in B6D2/F1 mice fed a 45% high-fat diet for 3 months ($n=12$ animals per group). **e**,**f**, Quantitative insulin-sensitivity check index (QUICKI) (**e**) and mRNA level of *Elovl6* (**f**) in response to refeeding in gonadal adipose tissue ($n=8$ animals per group) of C57BL/6J mice fed a 60% high-fat diet for 3 months ($n=8$ animals per group). **g–j**, Experiments were carried out in WT (white bars) and B6D2/F1 mice with zinc finger nuclease-mediated deletion of *Lipe* exon B; this promoter drives HSL expression in fat cells (*Lipe*$^{exonB-/-}$, grey bars). **g**, mRNA levels of transcripts containing different exons encoding HSL in inguinal adipose tissue ($n=12$ animals per group). **h**, Western blot analysis of adipose tissue HSL protein content (10 µg total protein) (WT $n=7$ animals; *Lipe*$^{exonB-/-}$ $n=5$ animals). GAPDH was used as western blot loading control. Size markers (in kDa) are shown on illustrative western blot panels. **i**, Plasma glucose concentration and area under the curve (AUC) during a glucose tolerance test (WT $n=7$ animals, *Lipe*$^{exonB-/-}$ $n=5$ animals) in mice fed a 60% high-fat diet for 3 weeks. **j**, mRNA level of adipose tissue *Elovl6* (WT $n=5$ animals, *Lipe*$^{exonB-/-}$ $n=6$ animals). Data are mean ± s.e.m. Statistical analysis was performed using Mann–Whitney test (**a–c**,**h–j**), unpaired Student's *t*-test (**e–g**) or two-way ANOVA with Bonferroni's post-hoc tests (**d**). Statistical tests were two-sided. *$P<0.05$ compared to control.

stem (hMADS) cells[12,13], HSL gene silencing (Supplementary Fig. 1a–c) increased insulin-stimulated glucose transport (Fig. 1a), glucose oxidation (Fig. 1b) and de novo lipogenesis (DNL) (Fig. 1c). Insulin signalling was enhanced in adipocytes with decreased HSL expression, as shown by enhanced activating phosphorylation of insulin receptor substrate 1 (IRS1), V-Akt murine thymoma viral oncogene homolog (AKT) and AKT substrate of 160 kDa (AS160) after insulin treatment (Fig. 1d–g). As adipose tissue DNL is associated with insulin sensitivity in humans[14,15], we tested whether direct inhibition of DNL affects the modulation of insulin signalling induced

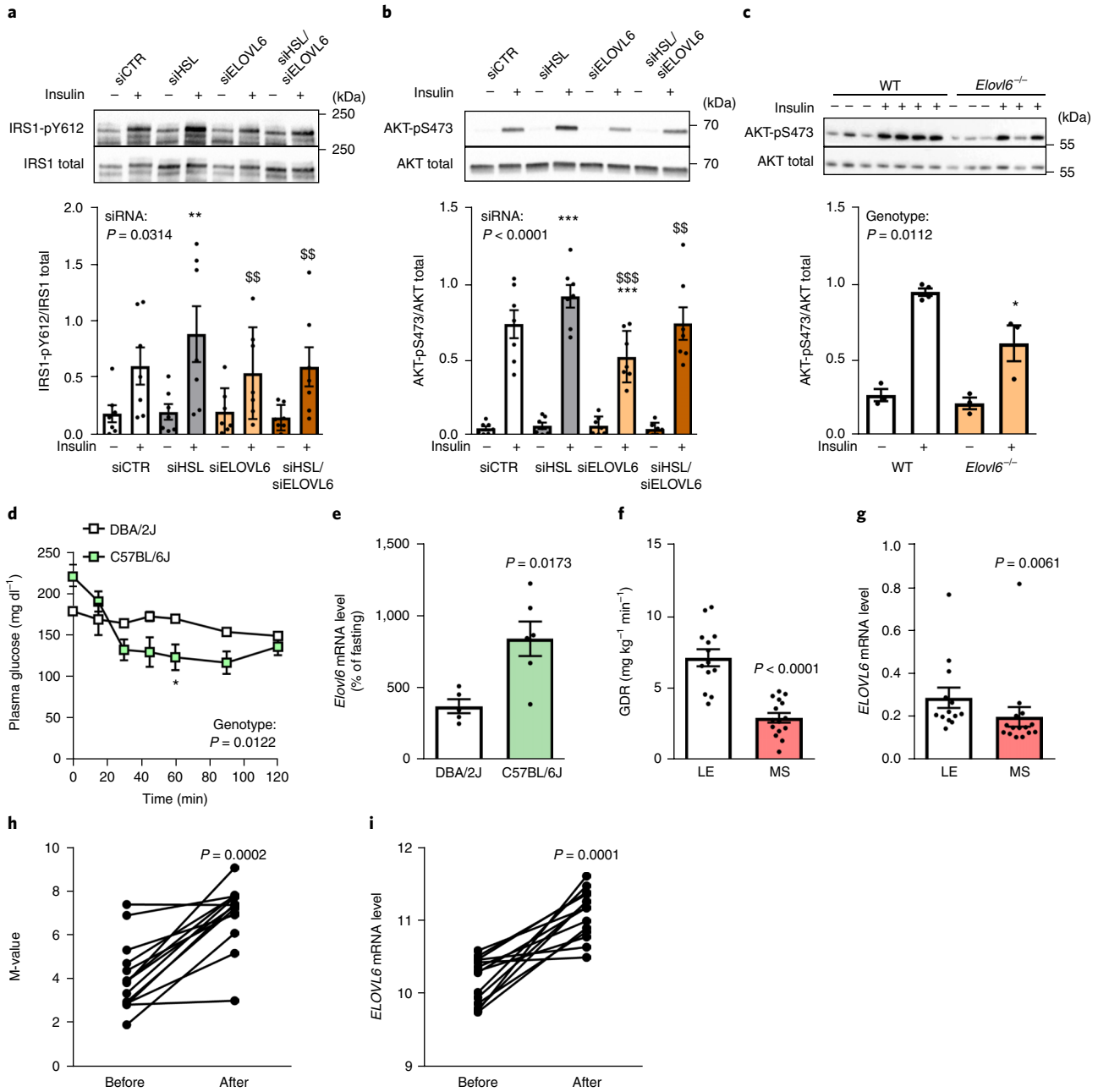

Fig. 3 | ELOVL6 has a positive effect on insulin signalling in adipocytes. a,**b**, Experiments were carried out in control (white bars, siCTR), single HSL (grey bars, siHSL), single ELOVL6 (light orange bars, siELOVL6) or dual HSL/ELOVL6-deprived (dark orange bars, siHSL/siELOVL6) hMADS adipocytes in basal (–) and insulin-stimulated (+, 100 nM) conditions. Insulin signalling evaluated by activating phosphorylation of IRS1 (pY612) ($n = 7$ biologically independent samples per group; insulin stimulation: $P = 0.0238$) (**a**) and AKT (pS473) ($n = 7$ biologically independent samples per group; insulin stimulation: $P < 0.0001$) (**b**). **c**, Insulin signalling evaluated by activating phosphorylation of AKT (pS473) in WT (white bars, $n = 4$ animals) and *Elovl6*-null (*Elovl6*$^{-/-}$, light orange bars, $n = 3$ animals) mice injected with a bolus of insulin (insulin stimulation: $P < 0.0001$). Size markers (in kDa) are shown on illustrative western blot panels. **d**,**e**, Plasma glucose concentration during an insulin tolerance test ($n = 9$ animals per group) (**d**) and gonadal adipose tissue *Elovl6* mRNA levels in response to refeeding (**e**) in DBA/2J (white bars, $n = 6$ animals) and C57Bl/6J (light green bars, $n = 5$ animals) mice. **f**,**g**, Glucose disposal rate (GDR) (**f**) and mRNA level of *ELOVL6* in visceral adipose tissue (**g**) from lean healthy (LE, white bars, $n = 13$ individuals) and obese women with metabolic syndrome (MS, light red bars, $n = 15$ individuals). **h**,**i**, Euglycemic-hyperinsulinemic clamp-derived M-value (**h**) and normalized *ELOVL6* mRNA level (**i**) in subcutaneous adipose tissue of obese women before and two years after bariatric surgery ($n = 14$ individuals). Data are mean ± s.e.m. Statistical analysis was performed using paired (**a**,**b**,**d**) and unpaired (**c**) two-way ANOVA with Bonferroni's post hoc tests, unpaired Student's *t*-test (**f**), Mann–Whitney test (**e**,**g**) and Wilcoxon's test (**h**,**i**). Statistical tests were two-sided. $^{*}P < 0.05$, $^{**}P < 0.01$, $^{***}P < 0.001$ compared to control condition or other mouse strain. In cell experiments, $^{\$\$}P < 0.01$, $^{\$\$\$}P < 0.001$ compared to HSL-deprived adipocytes.

by HSL depletion. Treatment of human adipocytes with a selective inhibitor of fatty acid synthase (Supplementary Fig. 1d) blunted the induction of insulin-mediated phosphorylation of AKT observed in HSL-deficient fat cells (Supplementary Fig. 1e). Furthermore, HSL inhibition decreased the proportion of palmitic acid and palmitoleic acid but increased that of oleic acid in fat cell triglycerides and

phospholipids (Fig. 1h,i). We thereby analyzed gene expression of enzymes catalyzing key steps in the synthesis of the main saturated and monounsaturated fatty acids derived from glucose in human fat cells (Supplementary Fig. 1d). In hMADS adipocytes with decreased HSL expression, the most robust induction was observed for *ELOVL6* (Fig. 1j). The increase in the *ELOVL6* mRNA level was mirrored by an increase in enzyme activity (Supplementary Fig. 1f) and an increase in the fatty acid elongation ratio attributable to ELOVL6 activity (Supplementary Fig. 1g). *ELOVL6* also showed the highest induction among DNL genes in human preadipocytes differentiated in primary cultures (Supplementary Fig. 1h). Next, we evaluated the effect of adipose triglyceride lipase (ATGL, which is encoded by *PNPLA2*) through *PNPLA2* gene silencing in hMADS adipocytes (Supplementary Fig. 1i,j). ATGL precedes HSL in the sequential breakdown of triglycerides during adipocyte lipolysis. ATGL knockdown had no effect on fat cell DNL (Supplementary Fig. 1k,l). Together, the results show that HSL depletion improves insulin signalling and promotes DNL and modification in fatty acid composition. These changes are associated with induction of the fatty acid elongase ELOVL6.

HSL inhibition results in increased adipose *Elovl6* in vivo. To probe changes in insulin sensitivity upon decreased HSL expression in vivo, we investigated different mouse transgenic models, genetic backgrounds and diets. Compared to obese wild-type littermates fed with a 60% high-fat diet, B6D2/F1 transgenic mice with *Lipe* haploinsufficiency[11] showed no difference in body weight or fat mass (Supplementary Fig. 2a,b). During euglycemic-hyperinsulinemic clamp, the glucose infusion rate tended to increase (Fig. 2a), there was no change in the rate of glucose disappearance (Fig. 2b) and insulin-mediated suppression of hepatic glucose production increased (Fig. 2c). In *Lipe* haploinsufficient B6D2/F1 mice fed a 45% high-fat diet, insulin tolerance increased, whereas body weight was not modified (Fig. 2d and Supplementary Fig. 2c). In *Lipe* haploinsufficient C57BL/6J mice fed a 60% high-fat diet, enhanced insulin sensitivity was confirmed (Fig. 2e) and adipose *Elovl6* gene expression level was higher (Fig. 2f). As in human adipocytes (Fig. 1j and Supplementary Fig 1h), the induction was more pronounced for *Elovl6* than for other lipogenic genes (Supplementary Fig. 2d). Using zinc finger nuclease–mediated gene editing, we generated a mouse model with HSL knockdown in adipose tissue and unaltered expression in liver (Fig. 2g,h and Supplementary Fig. 2e–g). Mice with zinc finger nuclease–mediated deletion of Lipe exon B ($Lipe^{exonB-/-}$) that were fed a high-fat diet showed increased glucose tolerance (Fig. 2i) without alteration of body weight (Supplementary Fig. 2h). Adipose *Elovl6* gene expression was higher in these mice than in wild-type littermates (Fig. 2j). Furthermore, chronic treatment with a specific inhibitor of HSL did not alter body weight (Supplementary Fig. 2i), improved insulin sensitivity (Supplementary Fig. 2j) and increased adipose *Elovl6* gene expression (Supplementary Fig. 2k). Therefore, both genetic and pharmacologic inhibition of HSL results in improved insulin sensitivity and enhanced *Elovl6* expression in adipose tissue in vivo.

Adipose ELOVL6 is associated with insulin sensitivity. Knockdown of ELOVL6 in human adipocytes led to a significant decrease in *ELOVL6* mRNA level and activity (Supplementary Fig. 3a,b). The increases in IRS1 (Fig. 3a) and AKT (Fig. 3b and Supplementary Fig. 3c) phosphorylation observed in HSL-deficient adipocytes were abrogated after concomitant gene silencing of *ELOVL6*. In agreement with data in human adipocytes, in vivo insulin-stimulated Akt phosphorylation was decreased in adipose tissue of *Elovl6*-null mice (Fig. 3c and Supplementary Fig. 3d,e). In mice fed a high-fat diet, C57BL/6J mice showed higher insulin tolerance (Fig. 3d and Supplementary Fig. 3f) and higher induction of adipose tissue *Elovl6* gene expression during refeeding than DBA/2J mice (Fig. 3e). In humans, adipose *ELOVL6* gene expression was lower in visceral adipose tissues of obese subjects with metabolic syndrome than in lean, insulin-sensitive individuals (Fig. 3f,g and Supplementary Fig. 3g). In morbidly obese subjects, weight loss observed 2 years after bariatric surgery (Supplementary Fig. 3h) was associated with greater insulin sensitivity (Fig. 3h) and an increase in subcutaneous adipose *ELOVL6* mRNA level (Fig. 3i). A strong positive correlation was found between *ELOVL6* mRNA levels and insulin sensitivity (Supplementary Fig. 3i). Taken together, the data identify ELOVL6 as the mediator of the beneficial effects of HSL inhibition and show a positive association between adipose *ELOVL6* expression and insulin sensitivity in vivo.

ELOVL6 controls plasma membrane fluidity. In triglycerides (Fig. 4a) and phospholipids (Fig. 4b) of human adipocytes, diminished ELOVL6 expression led to an increase in palmitic acid and palmitoleic acid at the expense of oleic acid. ELOVL6-deficient adipocytes showed a decrease in the proportion of oleic acid (for example, 36:2) and an increase in the proportion of palmitic acid (for example, 32:0) and palmitoleic acid (for example, 32:2) in phosphatidylcholines and phosphatidylethanolamines (Supplementary Fig. 4a–d). In vivo, the lack of *Elovl6* in mouse adipose tissue resulted

Fig. 4 | Oleic acid content in phospholipids and plasma membrane fluidity mediates the ELOVL6 positive effect on insulin signalling. a–h, Experiments were carried out in control (white bars, siCTR), single HSL (grey bars, siHSL), single ELOVL6 (light orange bars, siELOVL6) or dual HSL/ELOVL6-deprived (dark orange bars, siHSL/siELOVL6) hMADS adipocytes. **a**,**b**, Fatty acid composition in triglycerides (**a**) and phospholipids (**b**) ($n=6$ biologically independent samples per group). **c–f**, hMADS adipocytes were treated with vehicle (DMSO), 1 μM ELOVL6 inhibitor (ELOVL6i) or 75 nM SCD inhibitor (SCDi) for 48 h. Fatty acid ratios ($n=6$ for ELOVL6i and $n=5$ for SCDi biologically independent samples per group) (**c**,**e**) and insulin signalling evaluated by activating phosphorylation of AKT (pS473) in basal (−) and insulin-stimulated conditions (+, 100 nM) ($n=4$ biologically independent samples per group for ELOVL6i and SCDi; insulin stimulation: $P<0.0001$) (**d**,**f**). DMSO-treated adipocyte values are common to panels **d** and **f** and Supplementary Fig. 1e. **g**,**h**, hMADS were treated with vehicle (V), 100 μM (O100) or 500 μM (O500) of oleic acid for 48 h. Oleic acid levels in phospholipids ($n=5$ biologically independent samples per group) (**g**) and insulin signalling evaluated by activating phosphorylation of AKT (pS473) ($n=5$ biologically independent samples per group) in basal (−) or insulin-stimulated (+, 100 nM) conditions (insulin stimulation: $P=0.0003$) (**h**). For panels **d**,**f**,**h**, cropped images of vehicle and treatment lanes originate from the same blot. Size markers (in kDa) are shown on illustrative western blot panels. **i–l**, Experiments were carried out in control hMADS adipocytes expressing GFP (white bars, adeno-CTR) or overexpressing human ELOVL6 and GFP (avocado bars, adeno-ELOVL6). **i**,**j**, Fatty acid ratio ($n=8$ biologically independent samples per group) (**i**) and activating phosphorylation of IRS1 (pY612) in basal (−) and insulin-stimulated conditions (+, 100 nM) ($n=8$ biologically independent samples per group; insulin stimulation: $P<0.0001$) (**j**). **k**,**l**, FRAP experiments using fluorescent cholera toxin B (Alexa555-CTxB) ($n=5$ independent experiments). **k**, Representative confocal microscope image showing GFP and Alexa455-CTxB at room temperature of a successfully transduced hMADS adipocyte. Scale bar, 50 μm. **l**, Calculated mobile fraction (white bar, $n=17$ analyzed cells; avocado bar, $n=16$ analyzed cells). Data are mean ± s.e.m. Statistical analysis was performed using Wilcoxon's test (**a**,**b**), paired (**c–f**,**h**,**j**) and unpaired (**d**) two-way ANOVA with Bonferroni's post hoc tests, Friedman's with Dunn's post hoc tests (**g**), paired Student's *t*-test (**i**) and Mann-Whitney test (**l**). Statistical tests were two-sided. $^{*}P<0.05$, $^{**}P<0.01$, $^{***}P<0.001$ compared to control. $^{\$\$}P<0.01$, $^{\$\$\$}P<0.001$ compared to HSL-deprived adipocytes. $^{\#}P<0.05$, $^{\#\#}P<0.01$ compared to HSL- and ELOVL6-deprived adipocytes.

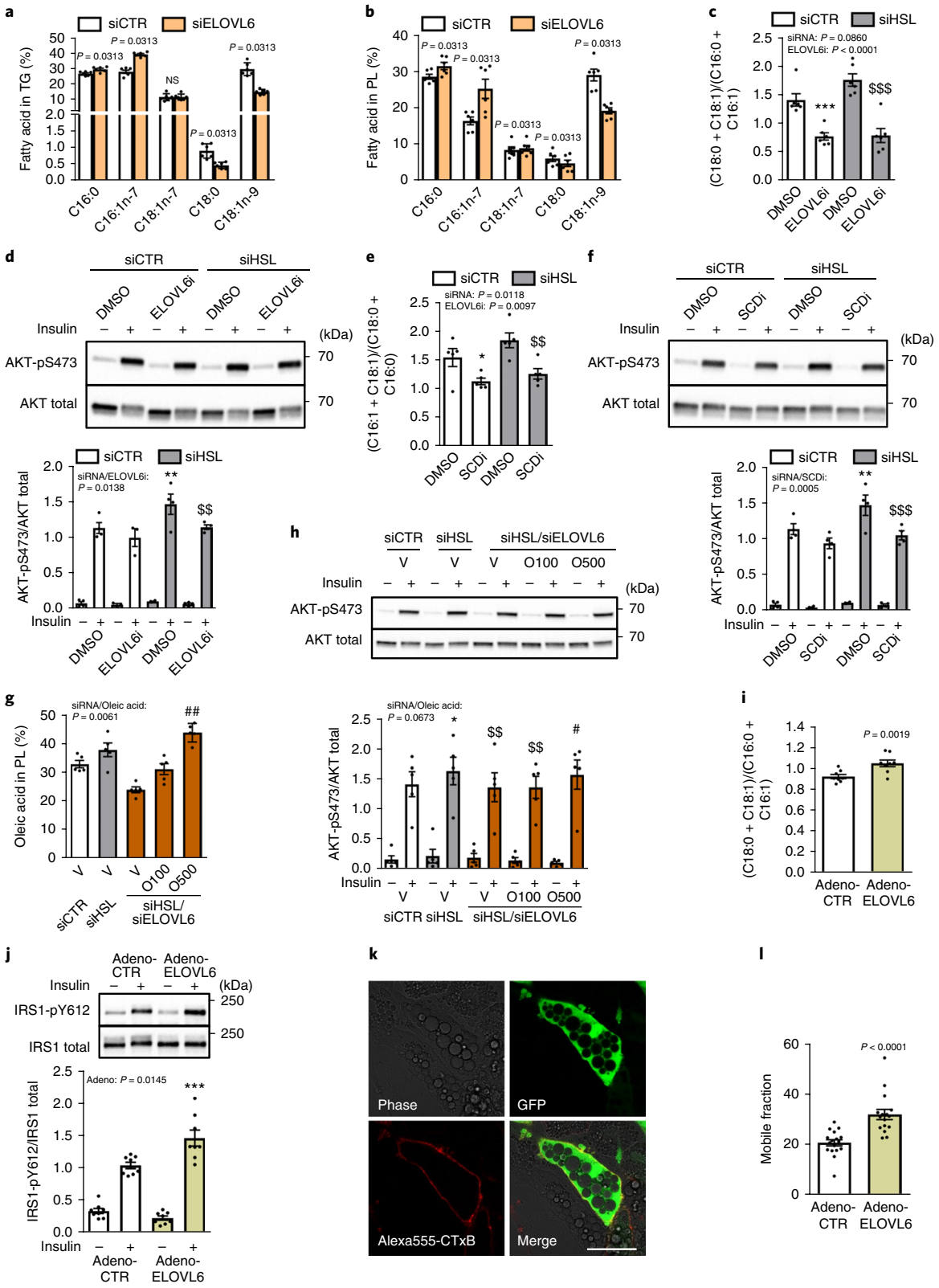

in increased palmitic and palmitoleic acid and decreased oleic acid content (Supplementary Fig. 4e). Considering that ELOVL6 mediates the positive effect of HSL gene silencing on insulin signalling (Fig. 3a,b and Supplementary Fig. 3c), we determined whether this effect was dependent on oleic acid. There are two enzymatic steps between palmitic acid and oleic acid (Supplementary Fig. 1d). The first is the elongation of palmitic acid into stearic acid catalysed by ELOVL6, and the second is the desaturation of stearic acid into oleic acid catalyzed by stearoyl-CoA desaturase (SCD)[16–19]. Treatment of human adipocytes with an inhibitor of ELOVL6 (ref. [20]) resulted in the changes we expected in fatty acid composition with a decrease of the C18/C16 fatty acid ratio (Fig. 4c). Concordant with data obtained using gene silencing (Fig. 3b), pharmacological inhibition of ELOVL6 abrogated the enhancement of insulin-induced AKT

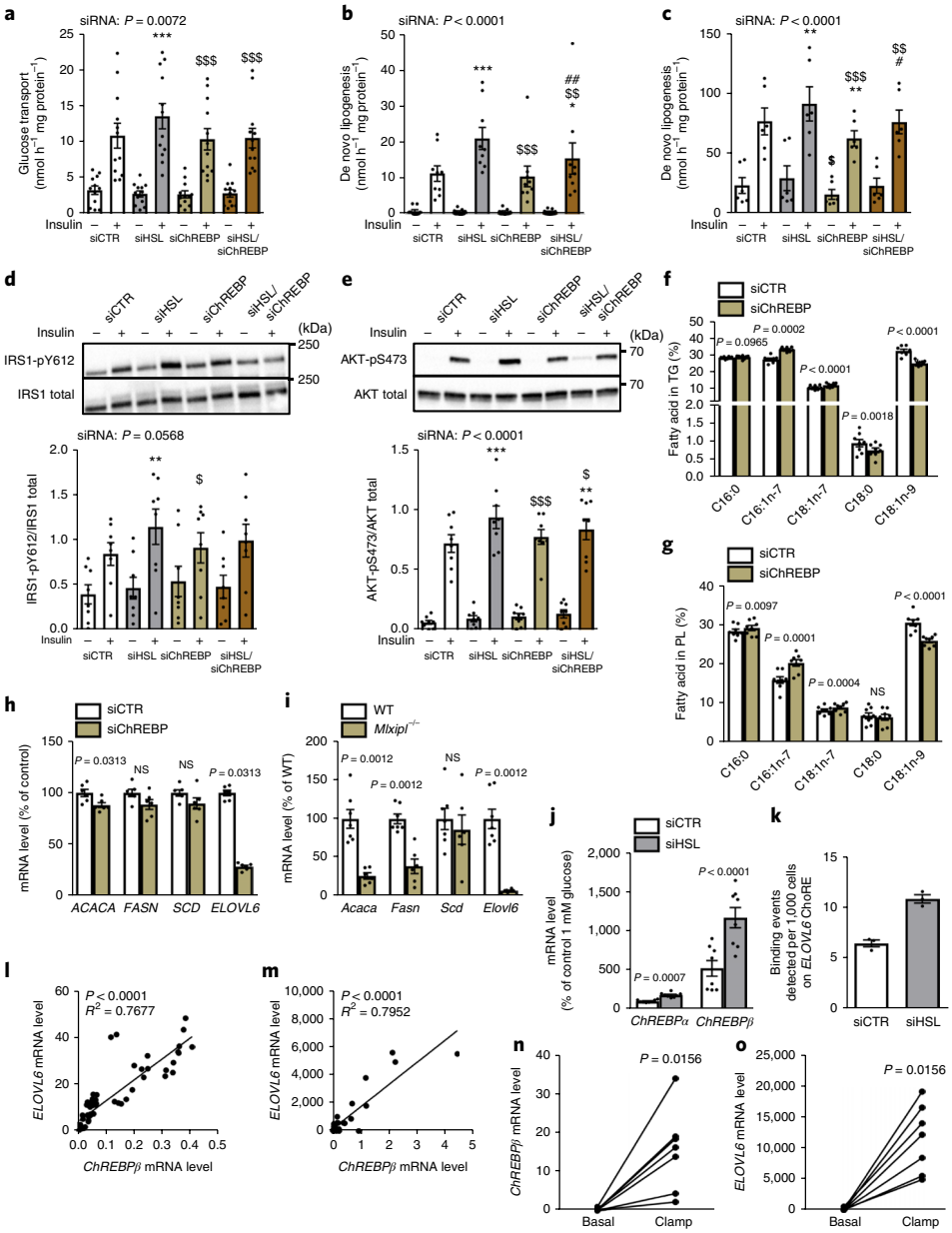

Fig. 5 | The glucose-sensitive transcription factor ChREBP mediates the beneficial effect of diminished HSL expression on glucose metabolism and insulin signalling in adipocytes. a–e, Experiments were carried out in control (white bars, siCTR), single HSL (grey bars, siHSL), single ChREBP (light brown bars, siChREBP) or dual HSL/ChREBP-deprived (dark brown bars, siHSL/siChREBP) hMADS adipocytes in basal (–) and insulin-stimulated (+, 100 nM) conditions. **a**, Glucose transport using radiolabelled 2-deoxyglucose ($n = 12$ biologically independent samples per group; insulin stimulation: $P < 0.0001$). **b**,**c**, DNL using radiolabelled glucose ($n = 9$ biologically independent samples per group; insulin stimulation: $P = 0.0002$) (**b**) or radiolabelled acetate ($n = 6$ biologically independent samples per group; insulin stimulation: $P = 0.0014$) (**c**). **d**,**e**, Insulin signalling evaluated by activating phosphorylation of IRS1 (pY612) ($n = 8$ biologically independent samples per group; insulin stimulation: $P = 0.0245$) (**d**) and AKT (pS473) ($n = 8$ biologically independent samples per group; insulin stimulation: $P < 0.0001$) (**e**). Size markers (in kDa) are shown on illustrative western blot panels. **f–h**, Experiments were carried out in control (white bars, siCTR) and ChREBP-deprived (light brown bars, siChREBP) hMADS adipocytes. **f**,**g**, Fatty acid composition in triglycerides (**f**) and phospholipids (**g**) ($n = 8$ biologically independent samples per group). **h**, mRNA levels of lipogenic enzymes ($n = 6$ biologically independent samples per group). **i**, mRNA levels of lipogenic enzymes in inguinal adipose tissue of wild-type (WT) (white bars, $n = 7$ animals) and *Mlxipl*-null mice (*Mlxipl*$^{-/-}$, light brown bars, $n = 6$ animals). **j**,**k**, Experiments were carried out in control (white bars, siCTR) and HSL-deprived (grey bars, siHSL) hMADS adipocytes cultivated in medium with 7.8 mM glucose and 10 nM insulin versus 1 mM glucose. **j**, Induction of mRNA levels encoding ChREBPα and ChREBPβ ($n = 8$ biologically independent samples per group). **k**, ChREBP recruitment on *ELOVL6* carbohydrate-responsive element (ChoRE) ($n = 3$ independent experiments). **l**,**m**, Correlations between mRNA levels of *ELOVL6* and ChREBPβ isoform in hMADS adipocytes ($n = 64$ biologically independent samples) (**l**) and in human subcutaneous adipose tissue ($n = 31$ individuals) (**m**). **n**,**o**, mRNA levels of *ChREBPβ* ($n = 7$ biologically independent samples per group) (**n**) and *ELOVL6* ($n = 7$ biologically independent samples per group) (**o**) in human subcutaneous adipose tissue in basal condition or during hyperglycemic-hyperinsulinemic clamp. Data are mean ± s.e.m. Statistical analysis was performed using paired two-way ANOVA with Bonferroni post hoc tests (**a–e**), paired Student's *t*-test (**f**,**g**,**j**), Wilcoxon's test (**h**,**n**,**o**), Mann–Whitney test (**i**) and linear regression (**l**,**m**). Statistical tests were two-sided. $^{*}P < 0.05$, $^{**}P < 0.01$, $^{***}P < 0.001$ compared to control. $^{\$}P < 0.05$, $^{\$\$}P < 0.01$, $^{\$\$\$}P < 0.001$ compared to HSL-deprived adipocytes. $^{\#}P < 0.05$, $^{\#\#}P < 0.01$ compared to ChREBP-deprived adipocytes.

phosphorylation observed in HSL-deficient adipocytes (Fig. 4d). A specific SCD inhibitor[21] decreased C16 and C18 fatty acid desaturation (Fig. 4e) and had the same effect as the ELOVL6 inhibitor on AKT phosphorylation (Fig. 4f). The data suggest that SCD is necessary but does not have a rate-limiting role, as ELOVL6 does, in increased insulin signalling induced by HSL inhibition. Accordingly, *SCD* mRNA levels are much higher than *ELOVL6* mRNA levels in human adipocytes (Supplementary Fig. 4f). The content of oleic acid in phospholipids was directly modified by incubation of adipocytes with the fatty acid (Fig. 4g). Exposure of HSL and ELOVL6 double-deficient adipocytes to oleic acid rescued insulin-induced AKT phosphorylation to levels comparable with those observed in fat cells with diminished HSL expression (Fig. 4h). The composition of fatty acid in phospholipids may influence insulin signal transduction through modification of plasma membrane properties[16,22,23]. Adenovirus-mediated overexpression of ELOVL6 in human adipocytes (Supplementary Fig. 4g,h) increased the C18/C16 fatty acid ratio (Fig. 4i) and insulin-induced IRS1 phosphorylation (Fig. 4j). Comparison of the mobile fractions derived from fluorescence recovery after photobleaching (FRAP) data revealed an increase in plasma membrane lateral mobility of cholera toxin–bound glycolipids in ELOVL6-overexpressing adipocytes (Fig. 4k,l). Collectively, the data suggest that enhanced adipocyte ELOVL6 activity increases the proportion of oleic acid in phospholipids and positively influences insulin signalling through modulation of plasma membrane fluidity.

ChREBP is the link between HSL and ELOVL6. During dual knockdown of HSL and ChREBP, encoded by *MLXIPL* (Supplementary Fig. 5a), the increase in glucose transport and DNL observed in adipocytes with low HSL expression was diminished (Fig. 5a–c). A similar pattern was observed for glucose and acetate carbon incorporation into fatty acid (Fig. 5b,c), showing that the upregulation of fatty acid synthesis resulted not only from increased glucose uptake but also from specific induction of DNL. *MLXIPL* gene silencing also mitigated the increase in insulin-induced IRS1 and AKT phosphorylation (Fig. 5d,e). Similar to what we observed for ELOVL6 knockdown (Fig. 4a,b), *MLXIPL* gene silencing led to an increase in palmitic acid and palmitoleic acid and a decrease of oleic acid (Fig. 5f,g). *MLXIPL* gene silencing potently suppressed *ELOVL6* gene expression but had a weak or no effect on other lipogenic genes, suggesting that ELOVL6 is a preferential target of ChREBP in human fat cells (Fig. 5h). Accordingly, in adipose tissue of *Mlxipl*-null mice (Supplementary Fig. 5b), *Elovl6* was the lipogenic gene whose expression was most severely impaired (Fig. 5i). Two isoforms of ChREBP have been identified: ChREBPα, whose transcriptional activity is regulated by glucose, and ChREBPβ, a transcriptionally superactive and unstable isoform that is a direct transcriptional target of ChREBPα (Supplementary Fig. 5c)[24,25]. In human adipocytes with knockdown of HSL, the levels of *MLXIPL* transcripts, notably that encoding the β-isoform of ChREBP, were increased (Fig. 5j). In chromatin immunoprecipitation assays on hMADS adipocytes, more binding events were detected on *ELOVL6* functional carbohydrate response element (ChoRE)[26] than on positive control regions in *RORC* and *TXNIP*, a well characterized target of ChREBP (Supplementary Fig. 5d). ChREBP recruitment onto the *ELOVL6* promoter was markedly enhanced in HSL-deficient adipocytes (Fig. 5k). *ELOVL6* was strongly associated with gene expression of ChREBPβ isoform transcripts in human adipocyte and human adipose tissue (Fig. 5l,m and Supplementary Fig. 5e,f). Short-term elevation in plasma glucose and insulin levels during a hyperglycemic hyperinsulinemic clamp led to pronounced induction of adipose ChREBPβ isoform transcript (Fig. 5n) and *ELOVL6* (Fig. 5o) gene expression, showing the importance of glucose flux into fat cells in the control of *ELOVL6* expression in humans. Altogether, our results show that ChREBPβ mediates the effect of HSL deficiency on glucose metabolism and insulin signalling through transcriptional activation of *ELOVL6*.

HSL modifies ChREBP activity via protein-protein interaction. Considering that HSL catalyzes one of the rate-limiting steps in fat-cell triglyceride hydrolysis, we investigated whether lipolysis per se contributed to the induction of ChREBP. In the culture conditions used to study DNL, the release of glycerol and fatty acid in the culture medium was low and was not influenced by HSL gene silencing (Supplementary Fig. 6a,b). Treatment of adipocytes with triacsin C,

Fig. 6 | HSL inhibits ChREBP activity through protein-protein interaction. a, Representative image of immunocomplexes between immobilized FLAG-ChREBPα and recombinant HSL (rec-HSL) ($n=3$ independent experiments). **b**, Representative surface plasmon resonance assay sensorgram showing binding of HSL to ChREBP. Purified ChREBP (220 RU) was first injected on a sensorchip with immobilized antibody to ChREBP. After ChREBP binding, the regulatory subunit of protein phosphatase 2A PR65α (no signal) and HSL (35 RU) were consecutively injected ($n=3$ independent experiments). **c**, Endogenous interaction between HSL and ChREBP in hMADS adipocytes ($n=3$ biologically independent samples per group). Anti-ChREBP was used for immunoprecipitation (IP). Normal rabbit IgG antibody was used as negative control. **d**, Endogenous interaction between HSL and ChREBP in white adipose tissue of *Lipe*$^{+/-}$ (+/−) and WT (+/+) mice ($n=4$ animals per group). Anti-ChREBP was used for immunoprecipitation. Rabbit IgG antibody was used as negative control. β-actin was used as western blot loading control. **e**, In situ proximity ligation assays (red signals) performed with anti-HSL and anti-ChREBP (PLA HSL/ChREBP) and corresponding image under visible light (phase) in control (siCTR) and HSL-deprived (siHSL) hMADS adipocytes. Nuclei were labelled in blue using 4,6-diamidino-2-phenylindole (DAPI). Representative image ($n=6$ independent experiments). Scale bars, 20 µm. **f**, Immunodetection of ChREBP (red) in control (siCTR) and HSL-deprived (siHSL) hMADS adipocytes. Representative image ($n=4$ independent experiments). Nuclei were labelled in blue using DAPI. Scale bars, 20 µm. **g**, ChREBPα protein levels in nuclear extracts from control (siCTR) and HSL-deprived (siHSL) hMADS adipocytes ($n=8$ biologically independent samples per group). **h**, ChREBPα protein levels in nuclear extracts from white adipose tissue of WT ($n=8$ animals) and *Lipe*$^{+/-}$ ($n=9$ animals) mice. **i**, Luciferase assays following transfection in HEK-293 cells of ChoREs fused to the luciferase gene along with expression vectors for ChREBP and HSL. ChoRE activity was measured in HEK-293 cells transfected with empty plasmid (pcDNA), ChREBP and different concentrations of HSL expression plasmids under low (5 mM) ($n=6$ biologically independent samples per group) and high (25 mM) glucose concentrations ($n=4$ biologically independent samples per group). **j**, HSL and ChREBPα immunocomplexes in HEK-293 cells transfected with empty plasmid (pcDNA), FLAG-ChREBP, full-length HSL (HSL) or short-form HSL (HSL-S) expression plasmids. Anti-FLAG was used for immunoprecipitation. β-actin was used as western blot loading control ($n=3$ independent experiments). **k**,**l**, Effect of overexpression of the short inactive form of HSL (HSL-S) in hMADS adipocytes. Experiments were carried out in control (siCTR, white bars) and HSL-deprived (siHSL, grey bars) hMADS adipocytes overexpressing GFP (Ad-CTR) or the short inactive form of HSL (Ad-HSL-S). **k**, mRNA levels of *ELOVL6* ($n=10$ biologically independent samples per group). **l**, Activating phosphorylation of IRS1 (pY612) in basal (−) and insulin-stimulated (+, 100 nM) conditions ($n=6$ biologically independent samples per group; insulin stimulation: $P<0.0001$). Size markers (in kDa) are shown on illustrative western blot panels. Data are mean ± s.e.m. Statistical analysis was performed using paired Student's *t*-test (**g**), Mann–Whitney test (**h**) or paired two-way ANOVA with Bonferroni's post-hoc tests (**i**,**k**,**l**). Statistical tests were two-sided. $^{*}P<0.05$, $^{**}P<0.01$ $^{***}P<0.001$ compared to ChREBP condition (**i**) or control adipocyte (**l**). $^{\$}P<0.05$, $^{\$\$\$}P<0.001$ compared to pcDNA condition (**i**) or siHSL/Ad-CTR adipocytes (**k**,**l**).

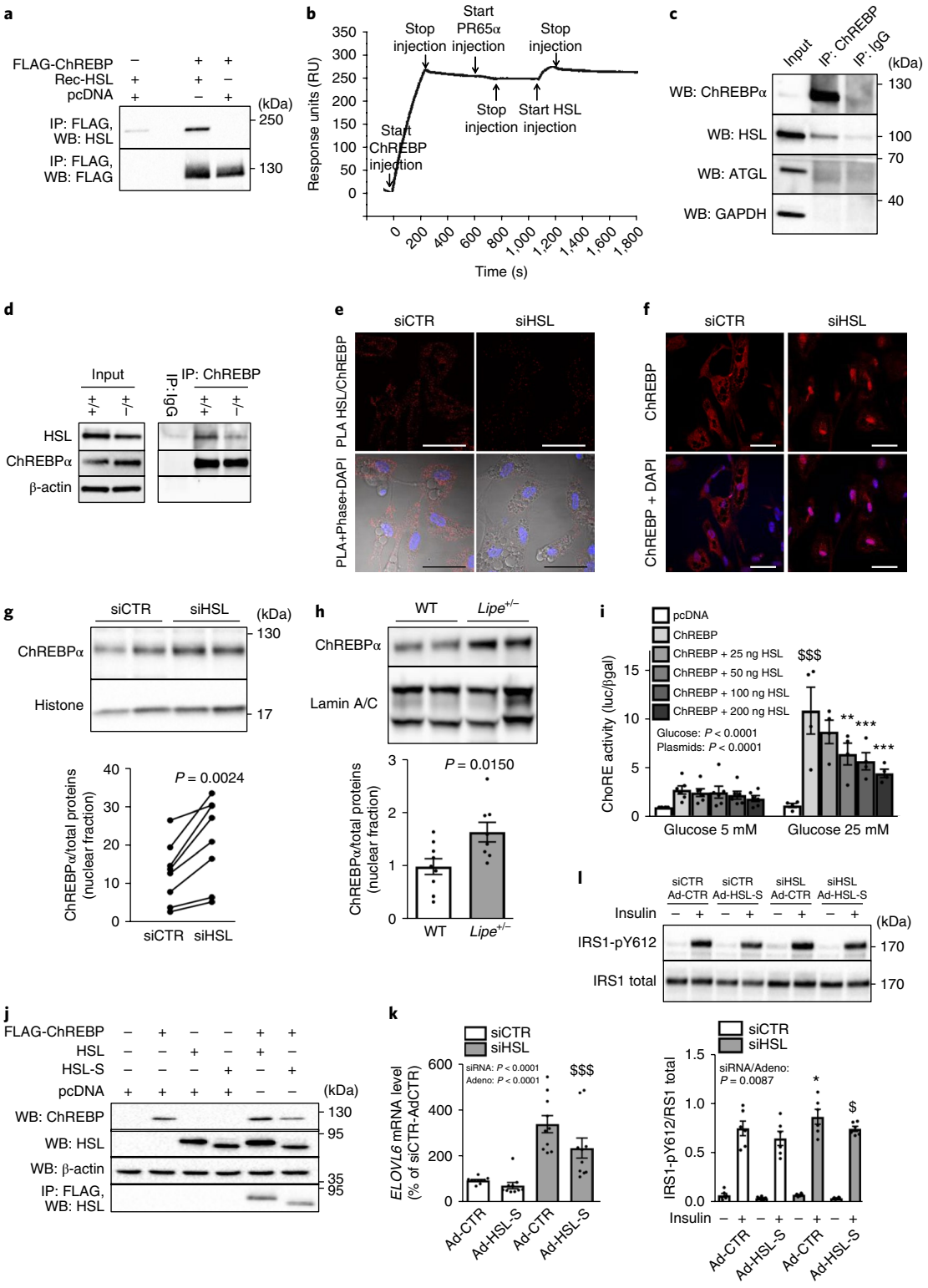

which inhibits fatty acid resterification[12] did not influence the upregulation of *MLXIPL* and *ELOVL6* mRNA in adipocytes with HSL knockdown (Supplementary Fig. 6c–e). These findings led us to hypothesize that physical interaction between HSL and ChREBP may influence ChREBP activity. Co-immunoprecipitation of HSL and ChREBPα was first shown in HEK293 cells transfected with vectors encoding the two proteins (Supplementary Fig. 6f)[27,28]. Co-immunoprecipitation was observed using ChREBPα with FLAG epitope tag immobilized on magnetic beads and recombinant HSL (Fig. 6a). Surface plasmon resonance assays supported direct binding between ChREBPα and HSL (Fig. 6b). Interaction between endogenous proteins in adipocytes was shown through immunoprecipitation with antibodies to ChREBP and HSL (Fig. 6c and Supplementary Fig. 6g). In line with the lack of effect of ATGL knockdown on DNL (Supplementary Fig. 1k,l), ATGL showed no interaction with ChREBPα. This further indicates that HSL interaction with ChREBPα is independent of lipolysis and specific to this neutral lipase (Fig. 6c). Furthermore, interaction of HSL with

ChREBPα was shown using in situ proximity ligation assays[29]. Specific and robust fluorescence signals were observed in the cytosol of fat cells from subcutaneous adipose tissue (Supplementary Fig. 6h). Such signals were also seen in differentiated hMADS adipocytes (Supplementary Fig. 6i). Little signal was detected in undifferentiated fibroblasts that do not express HSL. Various negative controls supported the specificity of the interaction (Supplementary Fig. 6j,k). Human HepG2 hepatocytes, which express significant levels of ChREBP but minute amounts of HSL, showed few fluorescent spots (Supplementary Fig. 6l,m). The respective expression of ChREBPα and HSL in mouse liver and adipose tissues is consistent with a fat-specific interaction of the two proteins (Supplementary Fig. 6n). In mouse adipose tissue and human adipocytes, co-immunoprecipitation and proximity ligation assay signal for HSL and ChREBP were diminished in fat cells with reduced HSL expression (Fig. 6d,e and Supplementary Fig. 7a). Human adipocytes with low HSL expression showed higher immunofluorescence of ChREBP in nuclei, indicating that ChREBPα nuclear translocation is facilitated when interaction with HSL is diminished (Fig. 6f). The increased nuclear translocation of ChREBPα was confirmed using subcellular fractionation in human adipocytes and mouse adipose tissues with low HSL expression, whereas no significant differences were observed in the cytosolic fraction (Fig. 6g,h and Supplementary Fig. 7b,c). In mice, there was no difference in ChREBPα protein content in fat pads with high and low HSL contents (Supplementary Fig. 7d). To evaluate the effect of HSL on ChREBPα transcriptional activity, HEK293 cells were transfected with a vector containing the luciferase reporter gene under the control of a promoter containing functional ChoREs[30]. Promoter activity increased when cells expressed ChREBPα and decreased when cells coexpressed increasing amounts of HSL (Fig. 6i and Supplementary Fig. 7e). When HEK293 cells expressing HSL and ChREBP were treated with a HSL inhibitor, less interaction between HSL and ChREBP was observed (Supplementary Fig. 7f). In human adipose tissue, we have previously identified a short form of HSL produced by in-frame skipping of exon 6 (Supplementary Fig. 2e)[31,32]. As exon 6 encodes the catalytic site serine, the short form of HSL is devoid of enzymatic activity (Supplementary Fig. 7g). However, it retains the capacity to bind ChREBP (Fig. 6j). An adenovirus expressing the short form of HSL was used to transduce human adipocytes transfected with control or *LIPE* small interfering RNA (siRNA) (Supplementary Fig. 7h). The induction of *ELOVL6* in adipocytes with diminished levels of HSL was blunted when the short form of HSL was expressed (Fig. 6k and Supplementary Fig. 7i). The catalytically inactive form also diminished the increase in IRS1 phosphorylation mediated by HSL downregulation (Fig. 6l). Notably, the changes in fat cell insulin signalling were not associated with variations in the amount of ChREBPα protein (Supplementary Fig. 7j,k). Together, our data suggest that HSL, independently of fat cell triglyceride hydrolysis, represses ChREBP activity via direct interaction with the transcription factor.

Discussion

Partial inhibition of the fat-cell neutral lipase HSL alleviates insulin resistance without increasing body weight (ref. [11] and present work). The evolution of plasma fatty acid levels and variation in insulin sensitivity were dissociated in this model. Here, we deciphered the mechanisms behind HSL inhibition–mediated improvement of glucose metabolism and identified interactions between prototypical metabolic pathways of the adipocyte (Supplementary Fig. 8).

Adipose DNL is under the control of the glucose-responsive transcription factor ChREBP. In humans, insulin sensitivity is positively associated with adipose DNL and expression of ChREBP, notably its transcriptionally superactive β-isoform[14,25,33,34]. Knockdown of ChREBP in human adipocytes counteracted effects of HSL gene silencing to increase insulin sensitivity. In this context, the fatty acid elongase ELOVL6 was the main target of ChREBPβ. We observed that *ELOVL6* expression in fat is lower in insulin-resistant than in insulin-sensitive subjects, in line with previous reports[14,35,36]. ELOVL6 catalyzes a critical step in the elongation of C16 fatty acid[19,37]. In adipocytes, enhanced ELOVL6 activity favored oleic acid synthesis whereas ELOVL6 knockdown had the opposite effect. In vivo and in vitro studies reveal a protective effect of oleic acid on insulin sensitivity and signalling[16,23,38,39]. As ELOVL6 induced an increase of oleic acid in major classes of phospholipids, we postulated that it may alter plasma membrane fluidity owing to its conformational plasticity[22,40,41]. The plasma membrane lateral mobility of glycolipids was increased in fat cells overexpressing ELOVL6. We therefore propose that ELOVL6-mediated increase in phospholipid oleic acid content improves fat cell insulin signalling through alteration of plasma membrane properties. In mice, *Elovl6* deficiency impaired white adipose tissue insulin signalling, whereas the opposite, or lack of alteration, has previously been reported in the liver, suggesting tissue-specific differences in ELOVL6-mediated modulation of insulin action[37,42].

HSL is a multifunctional enzyme with a broad range of substrates[43,44]. As ChREBP activity is influenced by metabolites and other transcription factors in the liver, products of HSL enzymatic activity could directly or indirectly influence ChREBP-mediated modulation of gene transcription[24]. Although we cannot rule out the possibility that, in some conditions, upregulation of ChREBPα protein expression partially contributes to the phenotype of adipocytes depleted in HSL, we bring a solid body of evidence showing that physical interaction between HSL and ChREBPα controls the intracellular location and activity of the transcription factor in fat cells. The catalytic activity of HSL is dispensable for the interaction with ChREBP and the ChREBP-mediated effect on *ELOVL6* expression and insulin signalling. A specific HSL inhibitor diminished the interaction between HSL and ChREBP and enhanced adipose *Elovl6* expression in mice, suggesting that small molecules may be designed to disrupt the interaction. The interaction between HSL and ChREBP, which controls ChREBP nuclear translocation and transcriptional activity, provides a molecular basis for the differences between liver and adipose tissue DNL. The pathway is generally considered as detrimental in the liver, as it is activated during the development of fatty liver disease, whereas it is seen as beneficial in adipose tissue[45,46]. Because of the low level of HSL expression, the interaction between HSL and ChREBP is not found in human hepatocytes. Alleviation of HSL-mediated inhibition of ChREBP activity may constitute a fat cell–specific mechanism to enhance DNL and insulin signalling.

In conclusion, our work identifies a pathway critical for optimal insulin signalling in fat cells that links the neutral lipase HSL to the glucose-responsive transcription factor ChREBP and its target gene, the fatty acid elongase *ELOVL6*. Inhibition of the HSL-ChREBP interaction may constitute an adipose-specific strategy to reduce insulin resistance.

Methods

General experimental approaches. No samples, mice, human research participants or data points were excluded from the reported analysis. Randomization was not performed except when noted below. Analyses were not blinded except when noted below. Detailed information and common techniques are described in Supplementary Methods as indicated below.

Culture of human adipocytes and in vitro measurements. *Culture of adipocytes.* hMADS cells were expanded in DMEM with 5.5 mM glucose (Lonza) supplemented with 10% FBS (Lonza), 2 mM L-glutamine (Invitrogen), 10 mM HEPES buffer (Lonza), 50 units ml^{-1} penicillin (Invitrogen) and 50 mg ml^{-1} streptomycin (Invitrogen), supplemented with 2.5 ng ml^{-1} fibroblast growth factor 2 (Sigma). At confluence, fibroblast growth factor 2 was removed from proliferation medium. On the next day (day 0), the cells were incubated in differentiation medium (DMEM and Ham's F-12 medium containing 7.8 mM glucose, HEPES, L-glutamine, penicillin-streptomycin, 10 μg ml^{-1} transferrin (Sigma), 10 nM insulin (Sigma), 0.2 nM triiodothyronine (Sigma), 100 μM 3-isobutyl-1-methylxanthine (Sigma), 1 μM dexamethasone (Sigma) and 100 nM rosiglitazone (Sigma)). At days

3 and 10, respectively, dexamethasone and 3-isobutyl-1-methylxanthine, and then rosiglitazone, were removed from culture medium. The experiments were carried out between days 12 and 15.

For primary culture and differentiation of human preadipocytes, subcutaneous adipose tissue samples were obtained from five women (age 39 ± 9 years; body mass index (BMI) 28 ± 4 kg m^{-2}) undergoing elective plastic surgery in the abdominal or dorsal region at Rangueil Hospital, Toulouse, France. Adipose tissue was cleaned from blood vessels and fibrous material, minced into pieces and digested in 1 volume of collagenase I (300 units ml^{-1}, Sigma) for 90 min in 37 °C shaking water bath. Digested tissue was filtered through a 250-µm strainer, diluted with PBS-gentamycin and centrifuged at 1,300 r.p.m. for 5 min. The pellet was incubated in erythrocyte lysis buffer for 10 min at room temperature. Cells were filtered, centrifuged and suspended in PM4 medium with 132 nmol l^{-1} insulin for differentiation and collected at day 13 (refs. [47,48]). The study was approved by the Ethics Committee of Toulouse University Hospitals (Comité de Protection des Personnes Sud Ouest et Outre Mer 2, DC-2014-2039). The volunteers signed informed consent for anonymous use of samples.

HEK293 and HepG2 cell cultures. See Supplementary Methods.

RNA interference. RNA interference was achieved by siRNA. Briefly, on day 7 and day 4 of differentiation, hMADS and primary preadipocytes, respectively, were detached from culture dishes with trypsin-EDTA (Invitrogen) and counted. Control siRNA against green fluorescent protein (GFP) (siCTR) and gene-specific siRNA for *LIPE*, *MLXIPL*, *ELOVL6* and *PNPLA2* (Eurogentec) were delivered into adipocytes using a microporator (Invitrogen) with the following parameters: 1,100 V, 20 ms and 1 pulse. The targeted sequences are provided in Supplementary Methods.

Adenoviral infection. Under the control of a cytomegalovirus promoter, adenoviruses encoding ELOVL6 in tandem with GFP (ADV-207862), the short form of HSL in tandem with GFP or encoding GFP alone (catalog no. 1060) were obtained from Vector Biolabs. Adenoviral particles (multiplicity of infection, 200) were added in the culture medium for 24 h at day 11–12 of hMADS cell differentiation. Medium was changed and experiments were carried out 48 h later.

Plasmid transfection. See Supplementary Methods.

Oleic acid supplementation in human adipocytes. See Supplementary Methods.

Treatments with enzyme inhibitors. For fatty acid synthase, SCD and ELOVL6 inhibition, hMADS adipocytes were treated, with 1 µM of compound AZ12756122 (example 117 from WO2008075070A1, synthesized at AstraZeneca), 75 nM of compound A939572 (ref. [21]) (Tocris Biosciences) and 1 µM compound 1w[20] (provided by AstraZeneca), respectively, in culture medium for 48 h. To study the effect of bioactive fatty acid on the induction of ChREBP, cells were treated for 8 h with 10 µM of triacsin C (Sigma), an inhibitor of acyl-CoA synthase, in the culture medium.

Gene expression analysis. See Supplementary Methods.

Characterization of human ChREBPβ-specific exon. See Supplementary Methods.

Western blot analysis. See Supplementary Methods.

Metabolic measurements. Triacylglycerol hydrolase activity was measured on cell extracts[12]. For other metabolic measurements, insulin was removed from culture medium the day before the assay. To determine glucose uptake, cells were incubated for 50 min at 37 °C with or without 100 nM insulin. Then, 125 µM of cold 2-deoxy-D-glucose and 0.4 µCi 2-deoxy-D-[^{3}H]glucose (PerkinElmer) per well were added for 10 min incubation. Culture plates were put on ice and rinsed with 10 mM glucose in ice-cold PBS and then with ice-cold PBS. Cells were scraped in 0.05 N NaOH, and radioactive 2-deoxy-D-glucose uptake was measured by liquid scintillation counting of cell lysate. To determine glucose oxidation, cells were incubated for 3 h in Krebs Ringer buffer supplemented with 2% BSA, 10 mM HEPES, 2 mM glucose and 1 µCi D-[^{14}C(U)]glucose (PerkinElmer) with or without 100 nM insulin. A 2- × 2-cm Whatman 3M paper was placed on top of each well and soaked with 120 µl 1 N NaOH. After incubation, filter-trapped $^{14}CO_2$ was measured by liquid scintillation counting. Medium was acidified with 1 M sulfuric acid and $^{14}CO_2$ in the culture medium was trapped by benzethonium hydroxide during a 2-h incubation. Benzethonium-trapped $^{14}CO_2$ was measured by liquid scintillation counting. Specific activity was counted and used to determine the quantity of oxidized glucose equivalent. To assess glucose incorporation into fatty acids, cells were then washed twice in PBS and then scraped in STED (0.25 mM sucrose, 10 mM Tris, 1 mM EDTA, 1 mM dithiothreitol, pH 7.4). Neutral lipids were extracted in methanol-chloroform (1:2). The organic phase was dried under nitrogen and hydrolyzed in 1 ml 0.25 N NaOH in methanol-chloroform (1:1) for 1 h at 37 °C. The solution was neutralized with 500 µl 0.5 N HCl in methanol. Fatty acids and glycerol were separated by adding 1.7 ml chloroform, 860 µl water and 1 ml methanol-chloroform (1:2). Incorporation of ^{14}C into fatty acids was measured by liquid scintillation counting of the lower phase. Specific activity was counted and used to determine the quantity of incorporated glucose equivalent. DNL was also measured using acetic acid-sodium salt-[1-^{14}C] (PerkinElmer). Cells were incubated for 3 h in Krebs buffer supplemented with 10 mM HEPES, 2 mM glucose, 2% BSA and 2 µCi ml^{-1} radiolabelled acetate stimulated with or without 100 nM insulin. Cells were then washed twice and harvested in PBS with 0.1% SDS. Neutral lipids were extracted in methanol–chloroform (1:2). Incorporation of ^{14}C into neutral lipids was measured by liquid scintillation counting of lower phase. Results from metabolic measurements were normalized to total protein content of cell extracts.

ELOVL6 activity. Fatty acid elongation activity was measured in crude microsomal extracts from hMADS adipocytes[37]. Briefly, cells were washed with PBS, scraped in 3 ml of ice-cold 250 mM sucrose, 20 mM HEPES, 1 mM EDTA, pH 7.5 and Dounce homogenized. Homogenate was centrifuged at 1,000*g* at 4 °C for 7 min. Supernatant was collected and centrifuged at 2,000*g* at 4 °C for 30 min. Supernatant was collected and centrifuged at 17,000*g* at 4 °C for 1 h. The resulting pellet was suspended in 50 µl of 100 mM Tris-HCl, pH 7.4, and used for fatty acid elongation activity after determination of protein concentration. ELOVL6 activity was assayed by the measurement of [2-^{14}C]malonyl-CoA (PerkinElmer) incorporation into exogenous palmitoyl-CoA[49]. ELOVL6 inhibitor (1 µM of compound 1w; ref. [20]) was preincubated for 30 min at 37 °C with microsomal protein before addition of reaction mixture. Incubation was stopped by adding 0.2 ml of 5 M KOH, 10% methanol, and saponified at 65 °C for 1 h. Then the samples were cooled and acidified with 0.2 ml of ice-cold 5 N HCl and 0.2 ml of ethanol. Free fatty acids were extracted from the mixture three times with 1 ml of hexane, 2% acetic acid. The pooled hexane fractions were dried under nitrogen, and after addition of 3 ml of scintillation cocktail, the radioactivity incorporated was counted. Blanks were carried out in parallel reactions incubated without microsomal fractions. ELOVL6 activity was obtained by subtracting [^{14}C]malonyl-CoA molecules incorporated into fatty acids in the absence of inhibitor from the values in the presence of the ELOVL6 inhibitor.

Chromatin immunoprecipitation assays. Human adipocyte cells (10^7 cells per condition) were fixed with 1% formaldehyde for 15 min and quenched with 0.125 M glycine. Chromatin was isolated by the addition of lysis buffer, followed by disruption with a Dounce homogenizer. Lysates were sonicated and the DNA sheared to an average length of 300–500 base pairs. Genomic DNA (Input) was prepared by treating aliquots of chromatin with RNase, proteinase K and heat for decrosslinking, followed by ethanol precipitation (Active Motif). Pellets were resuspended and the resulting DNA was quantified on a NanoDrop spectrophotometer. Extrapolation to the original chromatin volume allowed quantitation of the total chromatin yield. Aliquots of chromatin (30 µg) were precleared with protein A agarose beads (Invitrogen). Genomic DNA regions of interest were isolated using an antibody to ChREBP (Novus, NB400-135). Positive and negative controls were designed by Active Motif. Complexes were washed, eluted from the beads with SDS buffer and subjected to RNase and proteinase K treatment. Crosslinks were reversed by incubation overnight at 65 °C, and ChIP DNA was purified by phenol-chloroform extraction and ethanol precipitation. Quantitative PCR (qPCR) reactions were carried out in triplicate using SYBR Green Supermix (Bio-Rad, 170-8882) on a CFX Connect real-time PCR system. Positive and negative control sites were tested for each factor, and so were the sites of interest. The resulting signals were normalized for primer efficiency by carrying out qPCR for each primer pair using input DNA (pooled unprecipitated genomic DNA from each sample).

Cellular subfractionation. Nuclear and cytosolic fractions from hMADS adipocytes were prepared using Nuclear Extract Kit (40010) from Active Motif. Cells were rinsed with PBS and immediately scrapped into 1× hypotonic buffer. For adipose tissue, tissues were ground in liquid nitrogen and lysed using the NE-PER nuclear and cytoplasmic extraction reagent kit (Thermoscientific, 78835). Subsequent steps followed the manufacturer's protocol. Antibodies to histone H3 (4499, Cell Signaling Technology), lamin A/C (4777, Cell Signaling Technology) and α tubulin (T5168, Sigma) were used to analyze the efficiency of cellular fractionation.

Fatty acid composition of triglycerides and phospholipid. Cells were scraped in PBS and then mixed with methanol supplemented with 0.001% butylated hydroxytoluene. Lipid extraction was performed with a chloroform–methanol mixture (1:1) and KCl (0.5 M) after centrifugation (2,500 r.p.m., 10 min). Phospholipids and triglycerides were isolated by thin-layer chromatography on silica glass plates (Merck) using petroleum ether–diethyl ether–acetic acid (80:20:1) as the mobile phase. Fatty acid methyl esters were generated by transmethylation of the glycerolipids in methanol with 5% acetyl chloride at 60 °C for 1 h, extracted twice by isooctane. Analysis was carried out with a gas chromatograph (Shimadzu GC 2100) equipped with a CP-Wax 58 capillary column 50 m long with a 0.25-mm external diameter and 0.2-µm thickness of the stationary phase (Varian), with helium (1 ml min^{-1}) as the carrier gas. Programmed temperature vaporization (PTV system) injector and flame ionization detector were used. Results are expressed in percentage of total fatty acid contained in the sample.

Fatty acid composition in phospholipid classes. See Supplementary Methods.

Measurement of glycerol and NEFA in culture medium. See Supplementary Methods.

Fluorescence recovery after photobleaching. Cells were labelled for 15 min with 1 μg ml^{-1} Alexa 555-labelled Cholera ToxinSubunit B (CTxB Molecular Probes) at 4 °C, then washed three times in chilled medium supplemented with 25 mM HEPES buffer, pH 7.4. A LSM780 confocal microscope, equipped with highly sensitive 32-channel GaAsP detectors, operated with Zen Blue software, coupled to a DPSS laser (561 nm, maximum power 20 mW) was used for excitation with a detection bandwidth of 571–624 nm (Carl Zeiss). All experiments were done at room temperature (22 °C). Cells were observed using a Plan-Apochromat 63× NA, 1.4 oil immersion objective, and the pixel dwell was set to the optimal value of 1.92 μs. The fluorescence intensity of three regions of interest of 6.4 μm × 3.2 μm was measured: the photobleached area, a region within the cell that was not photobleached to check for overall photobleaching and cell position fluctuation, and the background. After 10 prebleach scans (one scan every 200 ms) at 1% maximal laser power to determine initial fluorescence intensity, one photobleaching scan was performed at 100% laser power. Postbleach fluorescence recovery was then sampled at 1% laser power for 150 s. FRAP data analysis was done as described by Bonneau et al[50].

Immunoprecipitation. HEK293T cells were harvested in a lysis buffer containing 3% 5 M NaCl, 5% 1 M Tris-HCl (pH 7.5), 1% 500 mM EDTA, 1.3% sodium pyrophosphate and 0.02% NaF, supplemented with 1% Triton X-100 (Sigma), 2% 50× protease inhibitor cocktail (Roche) and 1% 1 mM orthovanadate (Sigma). Protein (1 mg) was immunoprecipitated overnight at 4 °C, with 40 μl of anti-FLAG M2 magnetic beads (Sigma). Beads were gently centrifuged for 1 min and washed with the lysis buffer before elution in Laemmli buffer.

For immunoprecipitation of purified proteins, FLAG-tagged ChREBP was expressed in HEK293T cells. Cells were harvested in lysis buffer described above. Protein (300 μg) was immunoprecipitated overnight at 4 °C with 40 μl of anti-FLAG M2 magnetic beads. Beads bound with ChREBP were washed with the lysis buffer and incubated with 1 μg of human recombinant HSL (Cayman) in 350 μl of lysis buffer for 3 h at 4 °C with gentle rocking. The beads were washed three times with lysis buffer.

For endogenous co-immunoprecipitation in hMADS adipocytes, cells were lysed for 15 min in 1× hypotonic buffer (Active Motif) with 4% 25× protease inhibitor cocktail (Roche) and 1 mM orthovanadate (Sigma). Cell debris and fat were discarded after 12,700 r.p.m. centrifugation at 4 °C for 15 min. Preclearing was performed at 4 °C for 30 min using 50 μl protein G and 4 μg control rabbit (2729, Cell Signaling Technology) or mouse (sc-2025, Santa Cruz) IgG. Beads were discarded and supernatants were incubated with 4 μg anti-ChREBP (NB400-135, Novus) or 2 μg anti-HSL (sc-74489, Santa Cruz Biotechnology) for 90 min at 4 °C. As a negative control of immunoprecipitation, 4 μg control rabbit (2729, Cell Signaling Technology) or 2 μg mouse (sc-2025, Santa Cruz) IgG was used. Protein A–protein G (50:50) magnetic beads were added for 1 h at 4 °C. Beads were washed in cold PBS with 4% 25× protease inhibitor cocktail (Roche) and 1 mM orthovanadate.

For ChREBP immunoprecipitation in mouse white adipose tissue, fat was cut in small pieces and lysed during 2 h in 20 mM Tris-HCl, 150 mM NaCl, 0.5% NP-40 and protease and phosphatase inhibitors; pH 8. After centrifugation at 15,000*g* for 20 min at 4 °C, the fat layer was removed before collecting the supernatant. For each immunoprecipitation, 0.8–1 mg protein was precleared with 50 μl of Protein A Dynabeads (ThermoFisher) for 1 h at 4 °C, then incubated overnight at 4 °C with 40 μl Protein A dynabeads coupled with 5 μg rabbit IgG or ChREBP antibody (Novus). Beads were washed four times with lysis buffer before elution in 2× Laemmli buffer.

In situ proximity ligation assay and immunofluorescence. In situ proximity ligation assay was performed using Duolink In Situ reagents (Sigma). Cells and pieces of subcutaneous adipose tissue were fixed with 4% paraformaldehyde (Sigma) for 15 min and permeabilized for 10 min at room temperature with 0.2% Triton X-100 (Sigma). Incubation of antibodies, ligation of oligodeoxynucleotides and amplification were performed according to the manufacturer's instructions. The following primary antibodies were incubated overnight at 4 °C: anti-HSL (murine antibody, sc-74489, Santa Cruz Biotechnology), anti-ATGL (mouse antibody, NBP2-59390, Novus), anti-AKT (mouse antibody, 2920, Cell Signaling Technology) and anti-ChREBP (rabbit antibody, NB400-135, Novus). The same antibodies were used in immunofluorescence assays. Anti-mouse (Alexa-fluor 488-conjugated, A21202, and Alexa-fluor 546-conjugated, A10036, Invitrogen) and anti-rabbit (Alexa-fluor 546-conjugated, Invitrogen) secondary antibodies at 1/300 dilution were incubated for 45 min. Neutral lipids were stained using Bodipy (4-3922, Life Technologies) for 30 min. Nucleus labelling was done using Hoescht (33342, 5 mg ml^{-1}, Invitrogen) for 5 min. Confocal microscopy was performed using Zeiss LSM780. Image processing was similar for all conditions. The same settings were applied to entire images.

Surface plasmon resonance assays. All binding studies based on surface plasmon resonance technology were performed on a BIAcore T200 optical biosensor instrument (GE Healthcare). The Fc region of anti-ChREBP (NB400-135, Novus) was immobilized to the chip surface using native Protein A sensorchip in PBS-P+ buffer (20 mM phosphate buffer, pH 7.4, 2.7 mM KCl, 137 mM NaCl, and 0.05% surfactant P20) (GE Healthcare). Immobilization steps were performed at a flow rate of 5 μl min^{-1} with a final concentration of 2 μg ml^{-1}. Total amount of immobilized antibody was 11,000–12,000 response units (RU). Then all injection steps were performed at a flow rate of 20 μl min^{-1}. Channel Fc1 was used as a reference surface for nonspecific binding measurements.

Luciferase activity. See Supplementary Methods.

Animal studies. No randomization or blinding was performed. Animals from several litters were used in each protocol to avoid litter-to-litter variation.

Mouse models. Targeted disruption of the *Lipe* gene and generation of *Lipe*$^{+/-}$ mice have been described elsewhere[11]. Before being killed, mice were fasted for 24 h or re-fed for 18 h, supplemented with 20% glucose in drinking water. The promoter upstream of exon B governs HSL expression in fat cells[51]. To create transgenic mice with specific deletion of *Lipe* exon B, mRNA coding for zinc finger nucleases specifically targeting HSL (CompoZr Custom Zinc Finger Nucleases, CSTZFN-1KT, Sigma) was injected into pronuclei of one-cell embryos from female B6D2/F1 mice. Homozygous mice (*Lipe*$^{exonB-/-}$ registered as B6D2-*Lipe*^{em1Land} mice) were obtained. A full description of the model will be published elsewhere. The specific inhibitor of HSL (BAY 59-9435) was synthesized by NoValix[52]. Transgenic mice were fed a high-fat diet (60% or 45% kcal fat, respectively, D12492 and D12451 from Research Diets) for indicated times. In pharmacological studies, C57BL/6J male mice (12–15 weeks old, Janvier Laboratories) were treated orally with dimethylsulfoxide (DMSO) or HSL inhibitor (70 mg kg^{-1} once daily) for 11 d. Eight-week-old DBA2/J and C57BL6/J male mice (Charles River) were fed a high-fat diet (60% kcal fat, D12492 from Research Diets) for 6 weeks before being killed. Mice were housed and manipulated according to Inserm guidelines and European Directive 2010/63/UE in the local animal care facility (agreements A 31 555 04 and C 31 555 07). Protocols were approved by the French Ministry of Research after review by local ethical committee (CEEA122).

In studies on ChREBP-null mice, 10- to 12-week-old male and female *Mlxipl* global knockout mice[53] and wild-type littermates were maintained in a 12-h light, 12-h dark cycle with water and chow diet (65% carbohydrate, 11% fat and 24% protein). For the fasting–refeeding experiment, mice were either fasted for 24 h (fasted group) or re-fed for 18 h on chow diet with access to drinking water with 20% glucose after a 24-h fast (re-fed group). Mice were housed and manipulated according to Inserm guidelines and European Directive 2010/63/UE in the local animal care facility (agreement A751320). Protocols were approved by the French Ministry of Research after review by local ethical committee (CEEA34).

Mice homozygous for a deletion in *Elovl6* and their wild-type littermates were phenotyped on a C56BL6/J background[54]. The research has been regulated under the Animals (Scientific Procedures) Act 1986 Amendment Regulations 2012 after ethical review by the University of Cambridge Animal Welfare and Ethical Review Body.

Gene and protein expression analyses. See Supplementary Methods.

Measurement of fasting glucose and insulin. See Supplementary Methods.

Glucose and insulin tolerance tests and insulin bolus injection. See Supplementary Methods.

Euglycemic-hyperinsulinemic clamp. See Supplementary Methods.

Human research. The nature of the groups was blinded to the investigator performing gene expression experiments.

Women with differing obese and metabolic status. Participating women (lean group mean age 37 ± 16 years; obese with metabolic syndrome group mean age, 49 ± 11 years) were scheduled to have abdominal surgery (laparoscopic or laparotomic cholecystectomy and gastric banding)[55]. During the surgical procedure, samples of visceral adipose tissue were obtained by surgical excision. Euglycemic-hyperinsulinemic clamp was performed at rest after an overnight fast. Each subject gave written informed consent and the study was approved by the Ethics Committee of the Third Faculty of Medicine, Charles University, Prague.

Hyperglycemic-hyperinsulinemic clamp. The eight participating men were 23 ± 3 years old (body mass index (BMI) 23 ± 2 kg m^{-2}). The hyperglycemic hyperinsulinemic clamp was a modification of the hyperglycemic method used by Del Prato et al.[56] combined with the original hyperinsulinemic clamp described by Defronzo et al.[57] For hyperglycemia, the objective was to increase plasma glucose 5.5 mmol l^{-1} above fasting level by infusing 20% dextrose in two phases: (1) bolus dose to increase glycemia to the desired target and (2) continuous infusion dose adjusted every 5–10 min according to measured plasma glucose to maintain glycemia at the desired target. To obtain hyperinsulinemia, insulin was co-infused

at a rate of 75 mU m^{-2} min^{-1} for 180 min. The study was approved by the Ethics Committee of University of Montreal. The volunteers gave their written consent after being informed of the nature, purpose and possible risks of the study.

Morbidly obese subjects undergoing bariatric surgery. This cohort has in part been described before[58]. In brief, 14 obese women (BMI > 35 kg m^{-2}; age 48 ± 9 years) referred to the hospital for gastric bypass surgery (Roux-en-Y) were investigated before surgery and for 2 years post-operatively. According to self-report, body weight had been stable (±2 kg) for at least 3 months before both investigations. The study was approved by the regional ethics board in Stockholm and registered at http://clinicaltrials.gov as NCT01785134. Subjects were randomized to omentectomy or not and this was blinded to investigators and subjects. The procedure was explained in detail to each woman and written informed consent was obtained.

Gene expression analysis. See Supplementary Methods.

Statistical analysis. Results from biological replicates were expressed as mean ± s.e.m. Statistical analyses were performed using GraphPad Prism (GraphPad Software version 5.0). D'Agostino and Pearson omnibus normality test was used to test normality. Fischer test was used to test for equality of variances. Data were log transformed when appropriate to reach normality and uniform distribution. Statistical tests were two-sided. Paired or unpaired Student's *t*-tests, Wilcoxon test and Mann–Whitney test were performed to compare two conditions. Paired or unpaired one-way analysis of variance (ANOVA) and Friedman's tests were performed and followed by Bonferroni's and Dunn's post hoc tests, respectively, to determine differences between several groups. Paired or unpaired two-way ANOVA with Bonferroni's post hoc tests were used to compare two variables. Linear regression was used to test association between two variables.

Reporting Summary. Further information on research design is available in the Nature Research Reporting Summary linked to this article.

Data availability

The data that support the plots within this paper and other findings of this study are available from the corresponding author upon reasonable request.

Received: 15 May 2018; Accepted: 24 October 2018;
Published online: 03 December 2018

References

1. Abel, E. D. et al. Adipose-selective targeting of the GLUT4 gene impairs insulin action in muscle and liver. *Nature* **409**, 729–733 (2001).
2. Morley, T. S., Xia, J. Y. & Scherer, P. E. Selective enhancement of insulin sensitivity in the mature adipocyte is sufficient for systemic metabolic improvements. *Nat. Commun.* **6**, 7906 (2015).
3. Shearin, A. L., Monks, B. R., Seale, P. & Birnbaum, M. J. Lack of AKT in adipocytes causes severe lipodystrophy. *Mol. Metab.* **5**, 472–479 (2016).
4. Softic, S. et al. Lipodystrophy due to adipose tissue specific insulin receptor knockout results in progressive NAFLD. *Diabetes* **65**, 2187–2200 (2016).
5. Rondinone, C. M. et al. Insulin receptor substrate (IRS) 1 is reduced and IRS-2 is the main docking protein for phosphatidylinositol 3-kinase in adipocytes from subjects with non-insulin-dependent diabetes mellitus. *Proc. Natl Acad. Sci. USA* **94**, 4171–4175 (1997).
6. Carvalho, E., Jansson, P. A., Nagaev, I., Wenthzel, A. M. & Smith, U. Insulin resistance with low cellular IRS-1 expression is also associated with low GLUT4 expression and impaired insulin-stimulated glucose transport. *FASEB J.* **15**, 1101–1103 (2001).
7. Frojdo, S., Vidal, H. & Pirola, L. Alterations of insulin signaling in type 2 diabetes: a review of the current evidence from humans. *Biochim. Biophys. Acta* **1792**, 83–92 (2009).
8. Nyman, E. et al. A single mechanism can explain network-wide insulin resistance in adipocytes from obese patients with type 2 diabetes. *J. Biol. Chem.* **289**, 33215–33230 (2014).
9. Samuel, V. T. & Shulman, G. I. Mechanisms for insulin resistance: common threads and missing links. *Cell* **148**, 852–871 (2012).
10. Karpe, F., Dickmann, J. R. & Frayn, K. N. Fatty acids, obesity, and insulin resistance: time for a reevaluation. *Diabetes* **60**, 2441–2449 (2011).
11. Girousse, A. et al. Partial inhibition of adipose tissue lipolysis improves glucose metabolism and insulin sensitivity without alteration of fat mass. *PLoS Biol.* **11**, e1001485 (2013).
12. Bezaire, V. et al. Contribution of adipose triglyceride lipase and hormone-sensitive lipase to lipolysis in hMADS adipocytes. *J. Biol. Chem.* **284**, 18282–18291 (2009).
13. Barquissau, V. et al. White-to-brite conversion in human adipocytes promotes metabolic reprogramming towards fatty acid anabolic and catabolic pathways. *Mol. Metab.* **5**, 352–365 (2016).
14. Eissing, L. et al. De novo lipogenesis in human fat and liver is linked to ChREBP-beta and metabolic health. *Nat. Commun.* **4**, 1528 (2013).
15. Roberts, R. et al. Markers of de novo lipogenesis in adipose tissue: associations with small adipocytes and insulin sensitivity in humans. *Diabetologia* **52**, 882–890 (2009).
16. Collins, J. M., Neville, M. J., Hoppa, M. B. & Frayn, K. N. De novo lipogenesis and stearoyl-CoA desaturase are coordinately regulated in the human adipocyte and protect against palmitate-induced cell injury. *J. Biol. Chem.* **285**, 6044–6052 (2010).
17. Guillou, H., Zadravec, D., Martin, P. G. & Jacobsson, A. The key roles of elongases and desaturases in mammalian fatty acid metabolism: insights from transgenic mice. *Prog. Lipid Res.* **49**, 186–199 (2010).
18. Hodson, L. & Fielding, B. A. Stearoyl-CoA desaturase: rogue or innocent bystander? *Prog. Lipid Res.* **52**, 15–42 (2013).
19. Ohno, Y. et al. ELOVL1 production of C24 acyl-CoAs is linked to C24 sphingolipid synthesis. *Proc. Natl Acad. Sci. USA* **107**, 18439–18444 (2010).
20. Nagase, T. et al. Synthesis and biological evaluation of a novel 3-sulfonyl-8-azabicyclo[3.2.1]octane class of long chain fatty acid elongase 6 (ELOVL6) inhibitors. *J. Med. Chem.* **52**, 4111–4114 (2009).
21. Xin, Z. et al. Discovery of piperidine-aryl urea-based stearoyl-CoA desaturase 1 inhibitors. *Bioorg. Med. Chem. Lett.* **18**, 4298–4302 (2008).
22. Antonny, B., Vanni, S., Shindou, H. & Ferreira, T. From zero to six double bonds: phospholipid unsaturation and organelle function. *Trends Cell Biol.* **25**, 427–436 (2015).
23. Holzer, R. G. et al. Saturated fatty acids induce c-Src clustering within membrane subdomains, leading to JNK activation. *Cell* **147**, 173–184 (2011).
24. Filhoulaud, G., Guilmeau, S., Dentin, R., Girard, J. & Postic, C. Novel insights into ChREBP regulation and function. *Trends Endocrinol. Metab.* **24**, 257–268 (2013).
25. Herman, M. A. et al. A novel ChREBP isoform in adipose tissue regulates systemic glucose metabolism. *Nature* **484**, 333–338 (2012).
26. Bae, J. S., Oh, A. R., Lee, H. J., Ahn, Y. H. & Cha, J. Y. Hepatic Elovl6 gene expression is regulated by the synergistic action of ChREBP and SREBP-1c. *Biochem. Biophys. Res. Commun.* **478**, 1060–1066 (2016).
27. Langin, D., Laurell, H., Holst, L. S., Belfrage, P. & Holm, C. Gene organization and primary structure of human hormone-sensitive lipase: possible significance of a sequence homology with a lipase of Moraxella TA144, an antarctic bacterium. *Proc. Natl Acad. Sci. USA* **90**, 4897–4901 (1993).
28. Stoeckman, A. K., Ma, L. & Towle, H. C. Mlx is the functional heteromeric partner of the carbohydrate response element-binding protein in glucose regulation of lipogenic enzyme genes. *J. Biol. Chem.* **279**, 15662–15669 (2004).
29. Soderberg, O. et al. Direct observation of individual endogenous protein complexes in situ by proximity ligation. *Nat. Methods* **3**, 995–1000 (2006).
30. Lou, D. Q. et al. Chicken ovalbumin upstream promoter-transcription factor II, a new partner of the glucose response element of the L-type pyruvate kinase gene, acts as an inhibitor of the glucose response. *J. Biol. Chem.* **274**, 28385–28394 (1999).
31. Laurell, H. et al. Species-specific alternative splicing generates a catalytically inactive form of human hormone-sensitive lipase. *Biochem. J.* **328**, 137–143 (1997).
32. Ray, H. et al. The presence of a catalytically inactive form of hormone-sensitive lipase is associated with decreased lipolysis in abdominal subcutaneous adipose tissue of obese subjects. *Diabetes* **52**, 1417–1422 (2003).
33. Hoffstedt, J., Forster, D. & Lofgren, P. Impaired subcutaneous adipocyte lipogenesis is associated with systemic insulin resistance and increased apolipoprotein B/AI ratio in men and women. *J. Intern. Med.* **262**, 131–139 (2007).
34. Kursawe, R. et al. Decreased transcription of ChREBP-alpha/beta isoforms in abdominal subcutaneous adipose tissue of obese adolescents with prediabetes or early type 2 diabetes: associations with insulin resistance and hyperglycemia. *Diabetes* **62**, 837–844 (2013).
35. Nilsson, E. et al. Altered DNA methylation and differential expression of genes influencing metabolism and inflammation in adipose tissue from subjects with type 2 diabetes. *Diabetes* **63**, 2962–2976 (2014).
36. Soronen, J. et al. Adipose tissue gene expression analysis reveals changes in inflammatory, mitochondrial respiratory and lipid metabolic pathways in obese insulin-resistant subjects. *BMC Med. Genom.* **5**, 9 (2012).
37. Matsuzaka, T. et al. Crucial role of a long-chain fatty acid elongase, Elovl6, in obesity-induced insulin resistance. *Nat. Med.* **13**, 1193–1202 (2007).
38. Ryan, M. et al. Diabetes and the Mediterranean diet: a beneficial effect of oleic acid on insulin sensitivity, adipocyte glucose transport and endothelium-dependent vasoreactivity. *QJM* **93**, 85–91 (2000).
39. Salas-Salvado, J. et al. Reduction in the incidence of type 2 diabetes with the Mediterranean diet: results of the PREDIMED-Reus nutrition intervention randomized trial. *Diabetes Care* **34**, 14–19 (2011).
40. Ibarguren, M. et al. Partitioning of liquid-ordered/liquid-disordered membrane microdomains induced by the fluidifying effect of 2-hydroxylated fatty acid derivatives. *Biochim. Biophys. Acta* **1828**, 2553–2563 (2013).

41. Pietilainen, K. H. et al. Association of lipidome remodeling in the adipocyte membrane with acquired obesity in humans. *PLoS Biol.* **9**, e1000623 (2011).
42. Moon, Y. A., Ochoa, C. R., Mitsche, M. A., Hammer, R. E. & Horton, J. D. Deletion of ELOVL6 blocks the synthesis of oleic acid but does not prevent the development of fatty liver or insulin resistance. *J. Lipid Res.* **55**, 2597–2605 (2014).
43. Kraemer, F. B. & Shen, W. J. Hormone-sensitive lipase: control of intracellular tri-(di-)acylglycerol and cholesteryl ester hydrolysis. *J. Lipid Res.* **43**, 1585–1594 (2002).
44. Lafontan, M. & Langin, D. Lipolysis and lipid mobilization in human adipose tissue. *Prog. Lipid Res.* **48**, 275–297 (2009).
45. Czech, M. P. Cellular basis of insulin insensitivity in large rat adipocytes. *J. Clin. Invest.* **57**, 1523–1532 (1976).
46. Solinas, G., Boren, J. & Dulloo, A. G. De novo lipogenesis in metabolic homeostasis: more friend than foe?. *Mol. Metab.* **4**, 367–377 (2015).
47. Skurk, T., Ecklebe, S. & Hauner, H. A novel technique to propagate primary human preadipocytes without loss of differentiation capacity. *Obes. (Silver Spring)* **15**, 2925–2931 (2007).
48. Rossmeislova, L. et al. Weight loss improves the adipogenic capacity of human preadipocytes and modulates their secretory profile. *Diabetes* **62**, 1990–1995 (2013).
49. Moon, Y. A., Shah, N. A., Mohapatra, S., Warrington, J. A. & Horton, J. D. Identification of a mammalian long chain fatty acyl elongase regulated by sterol regulatory element-binding proteins. *J. Biol. Chem.* **276**, 45358–45366 (2001).
50. Bonneau, L. et al. Plasma membrane sterol complexation, generated by filipin, triggers signaling responses in tobacco cells. *Biochim. Biophys. Acta* **1798**, 2150–2159 (2010).
51. Grober, J. et al. Characterization of the promoter of human adipocyte hormone-sensitive lipase. *Biochem. J.* **328**, 453–461 (1997).
52. Langin, D. et al. Adipocyte lipases and defect of lipolysis in human obesity. *Diabetes* **54**, 3190–3197 (2005).
53. Iizuka, K., Bruick, R. K., Liang, G., Horton, J. D. & Uyeda, K. Deficiency of carbohydrate response element-binding protein (ChREBP) reduces lipogenesis as well as glycolysis. *Proc. Natl Acad. Sci. USA* **101**, 7281–7286 (2004).
54. Tan, C. Y. et al. Brown adipose tissue thermogenic capacity is regulated by Elovl6. *Cell Rep.* **13**, 2039–2047 (2015).
55. Klimcakova, E. et al. Worsening of obesity and metabolic status yields similar molecular adaptations in human subcutaneous and visceral adipose tissue: decreased metabolism and increased immune response. *J. Clin. Endocrinol. Metab.* **96**, E73–E82 (2011).
56. Del Prato, S. et al. Characterization of cellular defects of insulin action in type 2 (non-insulin-dependent) diabetes mellitus. *J. Clin. Invest.* **91**, 484–494 (1993).
57. DeFronzo, R. A., Tobin, J. D. & Andres, R. Glucose clamp technique: a method for quantifying insulin secretion and resistance. *Am. J. Physiol.* **237**, E214–E223 (1979).
58. Dahlman, I. et al. The fat cell epigenetic signature in post-obese women is characterized by global hypomethylation and differential DNA methylation of adipogenesis genes. *Int. J. Obes. (Lond.).* **39**, 910–919 (2015).

Acknowledgements

The authors acknowledge N. Venteclef (Centre de Recherche des Cordeliers, Paris) and J. Boucher (AstraZeneca, Göteborg, Sweden) for critical reading and comments on the manuscript. E. Courty and J. Personnaz participated in mouse studies during internship at I2MC. The GenoToul Animal Care, Anexplo, Imaging-TRI (especially F. Gaits-Iacovoni for helpful discussion) and Quantitative Transcriptomics facilities contributed to the work. This work was supported by Inserm, Paul Sabatier University, Fondation pour la Recherche Médicale (DEQ20170336720 to D.L.), Agence Nationale de la Recherche (ANR-12-BSV1-0025Obelip and ANR-17-CE14-0015Hepadialogue to D.L.), Région Midi-Pyrénées (OBELIP and ILIP projects to D.L.), FORCE/F-CRIN for clinical research on obesity, EU/EFPIA Innovative Medicines Initiative Joint Undertaking (EMIF grant 115372 to P.A., A.V.P. and D.L.) and AstraZeneca France (TALIP project to D.L.). D.L. is a member of Institut Universitaire de France.

Author contributions

P.M. and M. Houssier performed the majority of in vitro experiments and analyzed data with the contribution of A. Mairal, C.G., F.B., B.M., E.R., P.D.D., V. Sramkova, V.B., D.B., M.M., C.L., L.L., F.L. and M. Harms. P.M., M. Houssier, E. Mouisel, G.T., S.V., L.M., S.G., B.M.-R., T.S., H.G., C.H., A.V.P. and C.P. performed and analyzed in vivo data from mouse models. P.M., S.B., M.M., B.F., A.A., E. Meugnier, C.L., R.R.L., W.S., V. Stich, P.A., M.R., N.V. and H.V. performed and analyzed in vivo data in human clinical studies. S.C.-B., S.V. and J.B.-M. analyzed lipidomics data. A. Mazars and M.Z. performed and analyzed FRAP experiments. B.P., C.M., N.V., S.H. and H.V. interpreted the data. P.M., M. Houssier and D.L. conceived the study, interpreted the data and wrote the manuscript. D.L. supervised the study.

Competing interests

T.S. is an employee of Physiogenex. M. Harms and S.H. are employees of AstraZeneca. The other authors declare no competing financial and non-financial interests.

Additional information

Supplementary information is available for this paper at https://doi.org/10.1038/s42255-018-0007-6.

Reprints and permissions information is available at www.nature.com/reprints.

Correspondence and requests for materials should be addressed to D.L.

Publisher's note: Springer Nature remains neutral with regard to jurisdictional claims in published maps and institutional affiliations.

© The Author(s), under exclusive licence to Springer Nature Limited 2018

nature research

Corresponding author(s): Dominique Langin

Reporting Summary

Nature Research wishes to improve the reproducibility of the work that we publish. This form provides structure for consistency and transparency in reporting. For further information on Nature Research policies, see Authors & Referees and the Editorial Policy Checklist.

Statistical parameters

When statistical analyses are reported, confirm that the following items are present in the relevant location (e.g. figure legend, table legend, main text, or Methods section).

n/a	Confirmed
☐	☒ The exact sample size (*n*) for each experimental group/condition, given as a discrete number and unit of measurement
☐	☒ An indication of whether measurements were taken from distinct samples or whether the same sample was measured repeatedly
☐	☒ The statistical test(s) used AND whether they are one- or two-sided *Only common tests should be described solely by name; describe more complex techniques in the Methods section.*
☒	☐ A description of all covariates tested
☐	☒ A description of any assumptions or corrections, such as tests of normality and adjustment for multiple comparisons
☐	☒ A full description of the statistics including central tendency (e.g. means) or other basic estimates (e.g. regression coefficient) AND variation (e.g. standard deviation) or associated estimates of uncertainty (e.g. confidence intervals)
☐	☒ For null hypothesis testing, the test statistic (e.g. *F*, *t*, *r*) with confidence intervals, effect sizes, degrees of freedom and *P* value noted *Give P values as exact values whenever suitable.*
☒	☐ For Bayesian analysis, information on the choice of priors and Markov chain Monte Carlo settings
☐	☒ For hierarchical and complex designs, identification of the appropriate level for tests and full reporting of outcomes
☐	☒ Estimates of effect sizes (e.g. Cohen's *d*, Pearson's *r*), indicating how they were calculated
☐	☒ Clearly defined error bars *State explicitly what error bars represent (e.g. SD, SE, CI)*

Our web collection on statistics for biologists may be useful.

Software and code

Policy information about availability of computer code

Data collection	ChemiDoc MP and ChemiTouch (BioRad), Image Lab(version 6 Bio-Rad), Zen 2012 Blue edition (Carl Zeiss Microscopy)
Data analysis	Statistical analyses were performed using GraphPad Prism (GraphPad Software v.5.0).

For manuscripts utilizing custom algorithms or software that are central to the research but not yet described in published literature, software must be made available to editors/reviewers upon request. We strongly encourage code deposition in a community repository (e.g. GitHub). See the Nature Research guidelines for submitting code & software for further information.

Data

Policy information about availability of data

All manuscripts must include a data availability statement. This statement should provide the following information, where applicable:

- Accession codes, unique identifiers, or web links for publicly available datasets
- A list of figures that have associated raw data
- A description of any restrictions on data availability

The data that support the plots within this paper and other findings of this study are available from the corresponding author upon reasonable request.

Field-specific reporting

Please select the best fit for your research. If you are not sure, read the appropriate sections before making your selection.

☒ Life sciences ☐ Behavioural & social sciences ☐ Ecological, evolutionary & environmental sciences

For a reference copy of the document with all sections, see nature.com/authors/policies/ReportingSummary-flat.pdf

Life sciences study design

All studies must disclose on these points even when the disclosure is negative.

Sample size	Cell studies : No sample size calculation was performed. Reproducibility of measured effects is good (see also Replication below). For data on human adipocytes, survey of recent literature in top tier journals shows that sample sizes presented here are above what is reported. For HEK cells, data were obtained from different cell transfections. Animal studies : No sample size calculation was performed. For phenotypic analyses, we followed guidelines from Institut Clinique de la Souris (http://www.ics-mci.fr), Mouse Phenome Data Base (http://phenome.jax.org/) and International Mouse Phenotyping Consortium (http://www.mousephenotype.org/). Human studies : No sample size calculation was performed. Sample availability determined the numbers. In cross-sectional comparisons of the same population, our own DNA microarray data showed variation in adipose tissue gene expression comparing 8 individuals per group (Klimcakova et al 2011 J Clin Endocrinol Metab 96, E73). In longitudinal studies (paired analysis), power calculation shows that significant differences in adipose gene expression are observed with 6 individuals (Marques-Quinones et al 2010 Am J Clin Nutr 92, 975).
Data exclusions	Cell studies : No data exclusion Animal studies: No data exclusion if completion of the protocol Human studies : No data exclusion if completion of the protocol
Replication	Data reported in the manuscript are from biological replicates. Cell studies : In studies on human adipocytes, reproducibility of measured effects is high when replicates are performed on different wells from the same cell passage and donor. One of the determinants in variability of baseline values is the degree of fat cell differentiation. We systematically checked for high level of differentiation. Replicates were performed both between and within cell culture passages. In HEK293 cell experiments, several rounds of cell transfection were systematically performed. Animal studies. Animals from several litters were used in each protocol to avoid litter-to-litter variation. In studies on transgenic lines, attention was paid to distribution of transgenic and wild type siblings among litters. Several HSL transgenic models were explored to reach conclusions. No replication of experiments was performed except as indicated below. Differences in insulin sensitivity between wild type and HSL haploinsufficient mice were replicated using different techniques on several cohorts. Differences in insulin tolerance between vehicle- and HSL inhibitor-treated mice were replicated on several cohorts. This difference was also replicated for comparisons between DBA/2J and C57Bl/6J mice fed high fat diet. The lower amount of total and exonB containing HSL transcripts observed in inguinal white adipose tissue of mice with zinc finger nuclease-mediated deletion of Lipe exon B was confirmed in two other cohorts. The lack of variation in exon A containing transcripts was also confirmed. Human studies : No replication of studies was performed.
Randomization	Statement on randomization is included in the manuscript. Cell studies : No randomization. Animal studies : No randomization due to necessary prior knowledge of genotypes. Human studies : No randomization in group comparisons. Morbidly obese individuals were randomized to omentectomy or not.
Blinding	Statement on blinding is included in the manuscript. Cell studies : Experiments were not blinded. Animal studies. Experiments were not blinded. Nature of the groups was blinded to investigators performing phenotypic analyses. Human studies. Nature of the groups was blinded to the investigator performing gene expression experiments.

Reporting for specific materials, systems and methods

Materials & experimental systems

n/a	Involved in the study
☐	☒ Unique biological materials
☐	☒ Antibodies
☐	☒ Eukaryotic cell lines
☒	☐ Palaeontology
☐	☒ Animals and other organisms
☐	☒ Human research participants

Methods

n/a	Involved in the study
☒	☐ ChIP-seq
☒	☐ Flow cytometry
☒	☐ MRI-based neuroimaging

Unique biological materials

Policy information about availability of materials

Obtaining unique materials	All unique materials are readily available from the authors except compounds synthesized by AstraZeneca (ELOVL6 and FAS inhibitors).

Antibodies

Antibodies used	Rabbit polyclonal anti-phospho-tyrosine 612-IRS1, Invitrogen, 44816G, lot RB221097A, 1/1000 Rabbit monoclonal anti-phospho-serine 473-AKT, Cell Signaling Technology, 4060, clone D9E, lot 19, 1/1000 Rabbit monoclonal anti-phospho-threonine 308-AKT, Cell Signaling Technology, 2965, clone C31E5E, lot 10, 1/1000 Rabbit polyclonal anti-phospho-threonine 642-AS160, Cell Signaling Technology, 4288, lot 2, 1/500 Rabbit monoclonal anti IRS1, Cell Signaling Technology, 3407, clone D23G12, lot 6, 1/1000 Rabbit monoclonal anti AKT, Cell Signaling Technology, 4691, clone C67E7, lot 20, 1/1000 Rabbit polyclonal anti AKT, Cell Signaling Technology, 9272, lot 19, 1/1000 Rabbit monoclonal anti AS160, Cell Signaling Technology, 2670, clone C69A7, lot 4, 1/500 Rabbit polyclonal anti-HSL, Cell Signaling Technology, 4107, lot 3, 1/1000 Rabbit polyclonal anti-ATGL, Cell Signaling Technology, 2138, lot 4, 1/1000 Rabbit polyclonal anti-ChREBP, Novus, NB400-135, lot N-1, 1/1000 Rabbit monoclonal anti GAPDH, Cell Signaling Technology, 2118, clone 14C10, lot 8, 1/5000 Mouse monoclonal anti HSL, Santa Cruz Biotechnology, sc-74489, clone G-7, lot L0211, 1/1000 Rabbit monoclonal anti beta-actin, Cell Signaling Technology, 4970, clone 13E5, lot 11, 1/1000 Rabbit monoclonal anti-Histone H3, Cell Signaling Technology, 4499, clone D1H2, lot 1, 1/2000 Mouse monoclonal anti-alpha-Tubulin, Sigma Aldrich, T5168, clone B-5-1-2, lot 051M4771, 1/7000 Mouse monoclonal anti LaminA/C, Cell Signaling Technology, 4777, clone 4C11, lot 4, 1/1000 Mouse monoclonal anti AKT, Cell Signaling Technology, 2920, clone 40D4, lot 3, 1/1000 Mouse monoclonal anti-PEDF R/PNPLA2/ATGL, Novus, NBP2-59390, clone 18E6, lot A1648001 Direct-Blot HRP anti-FLAG Tag Antibody, BioLegend, clone L5, lot B211619, 1/2000 Normal Rabbit IgG, Cell Signaling Technology, 2729, lot 7 and 8 Normal Mouse IgG, Santa Cruz Biotechnology, sc-2025, lot J2015 Anti-rabbit IgG HRP-linked, Cell Signaling Technology, 7074, lot 24 and 25, 1/10000 Anti-mouse IgG HRP-linked, Cell Signaling Technology, 7076, lot 22, 1/10000 Anti-mouse IgG (H+L) Alexa-fluor 488-conjugated, Invitrogen, A21202, lot 1423052, 1/500 Anti-mouse IgG (H+L) Alexa-fluor 546-conjugated, Invitrogen, A10036, lot 771559, 1/500 Anti-rabbit IgG (H+L) Alexa-fluor 546-conjugated, Invitrogen, A11010, lot 1813035, 1/500
Validation	Validation data are shown for each antibody by the manufacturers who provide lists of publications. For each antibody, we checked in Western blot analyses that the detected band corresponded exactly to the reported molecular mass following gel migration.

Eukaryotic cell lines

Policy information about cell lines

Cell line source(s)	HEK293-T and HepG2 cells were from ATCC (CRL-3216 and HB-8065, respectively). Human multipotent adipose-derived stem (hMADS) cells, established from the prepubic fat pad of a 4-month-old male (hMADS-3), were used between passages 16 and 25. These cells display self-renewal capacity in vitro, exhibit a normal diploid karyotype and maintain the capacity to undergo differentiation into adipoctes even after extensive expansion. hMADS cells were directly provided by the laboratory of E.-Z. Amri (iBV, CNRS UMR 7277, INSERM U1091, University of Nice Sophia Antipolis, Nice, France).
Authentication	None of the cell lines has been authenticated.
Mycoplasma contamination	All cell lines were tested negative for Mycoplasma contamination.
Commonly misidentified lines (See ICLAC register)	No commonly misidentified cell lines were used.

Animals and other organisms

Policy information about studies involving animals; ARRIVE guidelines recommended for reporting animal research

Laboratory animals	The following mouse strains were used : DBA2/J (male), C57BL6/J (male), B6D2/F1 (male and female). Mice were investigated at 12-15 weeks.
Wild animals	The study did not involve wild animals.
Field-collected samples	The study did not involve samples collected from the field.

Human research participants

Policy information about studies involving human research participants

Population characteristics	Women with differing obese and metabolic status :lean group, age 37 ± 16 years; obese with metabolic syndrome group, age, 49 ± 11 years. Men undergoing hyperglycemic hyperinsulinemic clamp: age, 23 ± 3 years Morbidly women undergoing bariatric surgery: age, 48 ± 9 years; investigation before surgery and 2 years post-operatively.
Recruitment	Participants were recruited according to each protocol approved by local Ethics Commitees. The volunteers gave their written consent after being informed of the nature, purpose, and possible risks of the study. The authors in charge of exploitation of data derived from the clinical studies are aware of any bias in recruitment that could modify the reported conclusions.